



**HAL**  
open science

# Oscillons and quasibreathers in the $\varphi^4$ Klein-Gordon model

Gyula Fodor, Péter Forgács, Philippe Grandclément, István Rácz

► **To cite this version:**

Gyula Fodor, Péter Forgács, Philippe Grandclément, István Rácz. Oscillons and quasibreathers in the  $\varphi^4$  Klein-Gordon model. *Physical Review D*, 2006, 74, pp.124003. 10.1103/PhysRevD.74.124003 . hal-03732417

**HAL Id: hal-03732417**

**<https://hal.science/hal-03732417>**

Submitted on 30 Jul 2022

**HAL** is a multi-disciplinary open access archive for the deposit and dissemination of scientific research documents, whether they are published or not. The documents may come from teaching and research institutions in France or abroad, or from public or private research centers.

L'archive ouverte pluridisciplinaire **HAL**, est destinée au dépôt et à la diffusion de documents scientifiques de niveau recherche, publiés ou non, émanant des établissements d'enseignement et de recherche français ou étrangers, des laboratoires publics ou privés.

**Oscillons and quasibreathers in the  $\phi^4$  Klein-Gordon model**Gyula Fodor,<sup>1</sup> Péter Forgács,<sup>1,2</sup> Philippe Grandclément,<sup>2,3</sup> and István Rácz<sup>1</sup><sup>1</sup>MTA RMKI, H-1525 Budapest 114, P.O. Box 49, Hungary<sup>2</sup>LMPT, CNRS-UMR 6083, Université de Tours, Parc de Grandmont, 37200 Tours, France<sup>3</sup>LUTH, CNRS-UMR 8102, Observatoire de Paris-Meudon, place Jules Janssen, 92195 Meudon Cedex, France

(Received 14 August 2006; published 4 December 2006)

Strong numerical evidence is presented for the existence of a continuous family of time-periodic solutions with “weak” spatial localization of the spherically symmetric nonlinear Klein-Gordon equation in 3 + 1 dimensions. These solutions are “weakly” localized in space in that they have slowly decaying oscillatory tails and can be interpreted as localized standing waves (quasibreathers). By a detailed analysis of long-lived metastable states (oscillons) formed during the time evolution, it is demonstrated that the oscillon states can be quantitatively described by the weakly localized quasibreathers. It is found that the quasibreathers and their oscillon counterparts exist for a whole continuum of frequencies.

DOI: [10.1103/PhysRevD.74.124003](https://doi.org/10.1103/PhysRevD.74.124003)

PACS numbers: 04.25.Dm, 04.40.Nr, 11.10.Lm, 11.27.+d

**I. INTRODUCTION**

Nonlinear wave equations (NLWE) lie at the heart of many fields in physics including hydrodynamics, classical integrable systems, field theories, etc. Let us give a prototype class of NLWE for a real scalar field,  $\phi$ , in 1 +  $n$  dimensional space-time:

$$-\frac{\partial^2 \phi}{\partial t^2} + \Delta^{(n)} \phi = F(\phi), \quad \text{where } \Delta^{(n)} = \sum_{i=1}^n \frac{\partial^2}{\partial x_i^2}, \quad (1)$$

where the real function,  $F(\phi)$ , defining the theory is given, for example, as  $F(\phi) = \phi(\phi^2 - 1)$  for the “canonical”  $\phi^4$  model, and  $F(\phi) = \sin(\phi)$  for the sine-Gordon (SG) model.

A particularly interesting class of solutions of NLWE is the class of nonsingular ones exhibiting spatial localization. Such spatially localized solutions have finite energy and can correspond to static particlelike objects or to various traveling waves. In field theory, localized static solutions have been quite intensively studied in a great number of models in various space-time dimensions, see e.g. the recent book of Sutcliffe and Manton [1].

Spatially localized solutions with a nontrivial time dependence (i.e. not simply in uniform motion) of NLWE are much harder to find. In fact, the simple qualitative argument stating that “anything that can radiate does radiate,” indicates that the time evolution of well localized Cauchy data leads *generically* to either a *stable static* solution plus radiation fields, or the originally localized fields disperse completely due to the continuous loss of energy through radiation. Since Derrick-type scaling arguments exclude the existence of localized static solutions in scalar field theories given by Eq. (1) in more than two spatial dimensions, for  $n > 2$  one does not expect to find localized states at all at the end of a time evolution. Simplifying somewhat the above, one could say that in the absence of static localized solutions, localized initial data cannot stay forever localized. In fact, for localized initial data there is a time scale which is the crossing time,  $\tau_c$  (the time it takes for a wave propagating with characteristic speed to cross

the localized region), and *a priori* one would expect the rapid dispersion of initially localized Cauchy data within a few units of  $\tau_c$ . One of the rare examples of a time-periodic solution, staying localized forever is the famous “breather” in the 1 + 1 dimensional sine-Gordon (SG) model.

In the 1 + 1 dimensional canonical (with a double well potential)  $\phi^4$  theory the pioneering work, based on perturbation theory by Dashen, Hasslacher, and Neveu [2], indicated the possible existence of breatherlike solutions. A completely independent numerical study by Kudryavtsev [3] has also indicated that suitable initial data evolve into breather-type states. These results stimulated a number of investigations about the possible existence of nonradiative solutions in the 1 + 1 dimensional  $\phi^4$  model. After a long history Segur and Kruskal [4] and Vuillermot [5] have finally established that in spite of the above-mentioned perturbative and numerical indications time-periodic spatially localized finite energy solutions (breathers) do not exist. Even if genuine localized breathers in the 1 + 1 dimensional  $\phi^4$  model are absent, in view of the perturbative and numerical evidence for the existence of long-living states “close” to genuine breathers, it is a natural question how to describe them. Boyd has made a detailed study of time-periodic solutions which are only *weakly localized* in space (i.e. the field  $\phi$  possesses a slowly decreasing oscillatory tail) but as long as the amplitude of the oscillatory “wings” are small they still have a well-defined core. Boyd has dubbed such solutions “nanopterons” (small wings); we refer to his book for a detailed review [6].

Quite interestingly, Bogoluvskii and Makhankov have found numerical evidence for the existence of spatially localized breather-type states in the spherically symmetric sector of  $\phi^4$  theory in 3 + 1 dimensions [7]. These breatherlike objects observed during the time evolution of some initial data are called nowadays “oscillons.” Most of the observed oscillon states are unstable having only a *finite lifetime*. They lose their energy by radiating it (slowly) to

infinity. More recent investigations started by Gleiser [8,9] have revealed that oscillons do form in a fairly large class of scalar theories in various spatial dimensions via the collapse of field configurations (initial data) that interpolate between two vacuum states of a double well potential. Such a spherically symmetric configuration corresponds to a bubble, where the interpolating region is the bubble wall that separates the two vacuum states at some characteristic radius. These works have led to a renewed interest in the subject.

It has been found that oscillons have extremely long lifetimes which is already quite remarkable and makes them of quite some interest. These long-living oscillon states seem to occur in a rather generic way in various field theories involving scalar fields in even higher dimensional space-times [10] and according to [11] oscillons are also present in the non-Abelian SU(2) bosonic sector of the standard model of electroweak interactions at least for certain values of the pertinent couplings. Such oscillons might have important effects on the inflationary scenario [12] as they could form in large numbers retaining a considerable amount of energy. A slightly different mechanism for the formation of long-lived objects (quasilumps) during first order phase transitions has been investigated in [13]. In a recent study [14] of a 1 + 1 dimensional scalar theory on an expanding background exhibited very long oscillon lifetimes, while in Refs. [15,16] extremely long-living oscillons have been exhibited in a 1 + 2 dimensional sine-Gordon model.

The sophisticated numerical simulations by Honda and Choptuik of the Cauchy problem for spherically symmetric configurations in the  $\phi^4$  theory in 3 + 1 dimensions [17,18] have revealed some interesting new features of the oscillons. In particular, in Ref. [17] it has been found that by a suitable fine-tuning of the initial data the lifetime of the oscillons could be increased seemingly indefinitely, and it has been conjectured that actually an infinitely long lived, i.e. nonradiative, spatially localized solution exists. Furthermore, the existence of such a solution would even provide the explanation of the “raison d’être” and of the observed genericness of long-lived oscillons. The eventual existence of a nonradiative breather in this simple and “generic”  $\phi^4$  model in 3 + 1 dimensions would be clearly of quite some importance. It should be noted that, in quite a few spatially discrete models, localized time-periodic “discrete breathers” have been shown to exist and they are being intensively studied [19].

One of the motivations of our work has been to clarify if nonradiative breathers indeed exist and to find them directly by studying time-periodic solutions of the NLWE. Our numerical results led us to conclude that no localized (with finite energy) time-periodic solutions exist in the  $\phi^4$  model. On the other hand, this study has led us to understand the oscillon phenomenon better and we present a simple but quantitatively correct scenario explaining some

important properties of the oscillons (such as their existence and their long lifetimes). Our scenario is based on the existence of a special class of time-periodic solutions which are weakly localized in space. Such solutions (which have infinite energy) will be referred to as quasibreathers (QB).

In the present paper, we make a detailed study of oscillons in the (already much studied)  $\phi^4$  model in 3 + 1 dimensions. Using a previously developed and well tested time evolution code where space is compactified, thereby avoiding the problem of artificial boundaries [20] (see also [21]), we compute some long-time evolutions of Gaussian-type initial data. We observe that long-living (6000–7000 in natural units) oscillon states are formed from generic initial data. These oscillons radiate slowly their energy and for short (as compared to their total lifetime) time scales they can be characterized by a typical frequency,  $\omega$ . This frequency increases slowly during the lifetime of the oscillon and when  $\omega$  reaches a critical value  $\omega_c \approx 1.365$  there is a rapid decay. By fine-tuning the initial data, one can achieve that the oscillon state instead of rapidly decaying evolves into a near time-periodic state, whose frequency is nearly constant in time and  $1.365 < \omega < 1.412$ . The existence of such near-periodic states (referred to as resonant oscillons) has been already reported in Ref. [17], and we also observe an increase of the lifetime of these states without any apparent limit by fine-tuning the parameters of the initial data to more and more significant digits. There are, however, also some discrepancies. We find that clearly distinct near-periodic states for various values of the pulsation frequency  $1.365 < \omega < 1.412$  exist. According to our results, there is little doubt that for any value of  $\omega$  in this range a corresponding near-periodic oscillon state exists. Our data clearly shows that the near-periodic states also radiate, although very weakly. The radiation becomes weaker and weaker as  $\omega \rightarrow \sqrt{2}$ .

On the other hand, we have implemented a multidomain spectral method in order to find directly stationary, time-periodic solutions of the NLWE and compare them to the long-living oscillon states obtained from the time evolution. This makes it possible to attack the problem of finding directly the putative time-periodic breather(s). (One could easily generalize our method for the quasiperiodic case.) We find that there is a large family of time-periodic solutions which are only *weakly localized* in space, in that they have a well defined core, and an oscillatory tail decreasing as  $\propto 1/r$ . We single out a special family among them by minimizing the amplitude of their oscillatory tail. This definition comes close to minimizing the energy density of the oscillatory tail. These solutions are the closest to a breather and for that reason we call them quasibreathers. They seem to exist for any frequency,  $0 < \omega < \sqrt{2}$ , although in this paper we exhibit QBs only with  $1.30 < \omega < \sqrt{2}$ . The amplitude of the oscillatory tail of the QBs

becomes arbitrarily small as the frequency approaches the continuum threshold defined by the mass of the field,  $\omega \rightarrow \sqrt{2}$ . Our numerical evidence speaks clearly against the possible existence of a truly localized, breatherlike solution periodic in time, for the frequency range  $1.30 \leq \omega \leq 1.412$  contrary to the claims of Ref. [17]. In view of these conflicting numerical findings it is now highly desirable to try to find an analytical proof or disproof of the existence of a localized nonradiative solution to settle this issue. We do not expect the situation being qualitatively different from the  $1 + 1$  dimensional case, and although the proofs of Refs. [4,5] are not applicable for the  $3 + 1$  dimensional case, we see no reason that their negative conclusion would be altered.

More importantly, we believe to have made a step towards understanding the mechanism behind the existence of such long-living oscillonic states without the need to invoke genuine breather solutions, which even if they would exist would be clearly nongeneric, while the QBs seem to be generic. The total energy of the quasibreathers is divergent, due to the lack of sufficient (exponential) spatial localization, hence they are not of direct physical relevance. Nevertheless a careful numerical study shows that the *oscillons* produced during the time evolution of some suitable Cauchy data are quantitatively very well described by the *quasibreathers*. By comparing the Fourier decomposition of an oscillon state at some instant,  $t$  characterized by a frequency,  $\omega(t)$ , obtained during the time evolution with that of the corresponding QB, we have obtained convincing evidence that the localized part of the oscillon corresponds to the core of the QB of frequency  $\omega(t)$ . What is more, the oscillatory tail of the QB describes very well the standing wave part of the oscillon. Our oscillon scenario is based on this analysis and leads us to propose that any oscillon contains the core and a significant part of the oscillatory tail of the corresponding QB. The time evolution of an oscillon can be approximatively described as an adiabatic evolution through a sequence of QBs with a slowly changing frequency  $\omega(t)$ . This oscillon scenario is based on the existence and of the genericness of the QBs.

Although in this paper we have investigated a specific  $\phi^4$  theory in  $3 + 1$  dimensions with spherical symmetry, we expect that our main results remain true in other theories without any restriction on the symmetry properties of the configurations, i.e. in general oscillons correspond to spatially cut off QB's. In view of the results of Ref. [22] indicating that nonsymmetric oscillons evolve towards symmetric ones (at least in  $1 + 2$  dimensions), we expect that the long time evolutions will be dominated by spherically symmetric configurations.

This paper is organized as follows. In Sec. II we study the time evolution of localized, Gaussian-type initial data in  $\phi^4$  theory and investigate some important aspects of the oscillon solutions. In Sec. III we present an infinite system

of coupled ordinary differential equations (ODE's) obtained by the Fourier-mode decomposition of the NLWE Eq. (3) and discuss some of its properties. Section IV is devoted to the description of the spectral methods used to solve this system. In particular, we carefully deal with the asymptotic behavior of the Fourier modes. Various convergence tests are exhibited. The quasibreathers are discussed in Sec. V, the results on our oscillon scenario are discussed in Sec. VI, and conclusions are drawn in Sec. VII.

## II. TIME EVOLUTION

### A. The nonlinear wave equation of the $\phi^4$ theory

We consider the following  $\phi^4$  theory in  $1 + 3$  dimensions whose action can be written as

$$S = \int dt d^3x \left[ \frac{1}{2}(\partial_t \phi)^2 - \frac{1}{2}(\partial_i \phi)^2 - \frac{1}{4}(\phi^2 - 1)^2 \right], \quad (2)$$

where  $\phi$  is a real scalar field,  $\partial_t = \partial/\partial t$ ,  $\partial_i = \partial/\partial x^i$ , and  $i = 1, 2, 3$ . In this paper we shall restrict ourselves to spherically symmetric field configurations, when the corresponding NLWE is given by

$$-\phi_{,tt} + \Delta \phi = \phi(\phi^2 - 1), \quad \text{where } \Delta = \partial_r^2 + \frac{2}{r} \partial_r. \quad (3)$$

The energy corresponding to the action (2) can be written as

$$E = 4\pi \int_0^\infty dr r^2 \xi, \quad (4)$$

where  $\xi$  denotes the energy density

$$\xi = \frac{1}{2}(\partial_t \phi)^2 + \frac{1}{2}(\partial_r \phi)^2 + \frac{1}{4}(\phi^2 - 1)^2. \quad (5)$$

It is easy to see that the finiteness of the total energy is guaranteed by  $\phi \rightarrow \pm 1 + \mathcal{O}(r^{-3/2})$  as  $r \rightarrow \infty$ .

### B. Numerical techniques

We briefly outline here the main ideas for the implementation of our evolution code to solve numerically the Cauchy problem for Eq. (3). Assuming  $\phi \rightarrow 1$  as  $r \rightarrow \infty$ , we introduce the new field  $\hat{\phi}$  as

$$\phi(t, r) = \frac{\hat{\phi}(t, r)}{r} - 1. \quad (6)$$

Then the NLWE Eq. (3) takes the form

$$r^2(\partial_r^2 \hat{\phi} - \partial_t^2 \hat{\phi}) = \hat{\phi}(\hat{\phi} - r)(\hat{\phi} - 2r). \quad (7)$$

The next step is to compactify in the spacelike directions by a suitable coordinate transformation of  $r$ . This way we can guarantee that our computational grid, associated with a finite-difference scheme, covers the entire physical space-time, at least in principle. Specifically, a new radial

coordinate,  $R$ , is introduced in the following way:

$$r = \frac{2R}{\kappa(1 - R^2)}, \quad (8)$$

where  $\kappa$  is an arbitrary positive constant. In the new radial coordinate,  $R$ , the entire Minkowski space-time is covered by the coordinate domain  $0 \leq R < 1$  while spacelike infinity is represented by the ‘‘hypersurface’’  $R = 1$ . The  $R = \text{const}$  ‘‘lines’’ represent world lines of ‘‘static observers,’’ i.e. integral curves of the vector field  $(\partial/\partial t)^a$ . In the compactified representation the field equation, (7), reads as

$$\begin{aligned} R^2 \left( \frac{4\Omega^4}{\kappa^2(1 + R^2)^2} \partial_R^2 \hat{\phi} - \partial_t^2 \hat{\phi} - \frac{4\Omega^3 R(R^2 + 3)}{\kappa(1 + R^2)^3} \partial_R \hat{\phi} \right) \\ = \hat{\phi}(\Omega \hat{\phi} - R)(\Omega \hat{\phi} - 2R), \end{aligned} \quad (9)$$

where  $\Omega$  is given by

$$\Omega = \frac{\kappa}{2}(1 - R^2). \quad (10)$$

We remark that the spacelike compactification used here is a simplified variant of the conformal transformation used in [20,21]. There instead of the  $t = \text{const}$  hypersurfaces the initial data are specified on hyperboloids. Furthermore, Minkowski space-time is compactified mapping null infinity to finite coordinate values. Since in the present case the scalar field,  $\phi$ , is massive, i.e. never reaches null infinity, the hyperboloidal compactification is not essential.

In order to obtain a system of first order equations we introduce the independent variables  $\hat{\phi}_t = \partial_t \hat{\phi}$  and  $\hat{\phi}_R = \partial_R \hat{\phi}$ . Then Eq. (9) can be rewritten as

$$\begin{aligned} \partial_t \hat{\phi}_t = \frac{4\Omega^4}{\kappa^2(1 + R^2)^2} \partial_R \hat{\phi}_R - \frac{4\Omega^3 R(R^2 + 3)}{\kappa(1 + R^2)^3} \hat{\phi}_R \\ + \hat{\phi} \left( \frac{\Omega}{R} \hat{\phi} - 1 \right) \left( \frac{\Omega}{R} \hat{\phi} - 2 \right), \end{aligned} \quad (11)$$

which together with the integrability condition  $\partial_t \hat{\phi}_R = \partial_R \hat{\phi}_t$  and the defining equation  $\partial_t \hat{\phi} = \hat{\phi}_t$  form a strongly hyperbolic system of first order differential equations for the three variables  $\hat{\phi}$ ,  $\hat{\phi}_t$ , and  $\hat{\phi}_R$  (see e.g. [23]). The initial value problem for such a first order system is known to be well-posed [24]. Note that the relation  $\partial_R \hat{\phi} = \hat{\phi}_R$  is preserved by the evolution equations, and therefore it corresponds to a constraint equation.

In order to solve the initial value problem for Eq. (11), we discretize the independent variables  $t$  and  $R$ . A simple uniform grid with steps  $\Delta t$  and  $\Delta R$  is introduced. Spatial derivatives are calculated by symmetric fourth order stencils. Time integration is done using the ‘‘method of lines’’ in a fourth order Runge-Kutta scheme, following the recipes proposed by Gustafsson *et al.* [24]. A dissipative term proportional to the sixth derivative of the field is added in order to stabilize the evolution. Since this dissipative term is also chosen to be proportional to  $(\Delta R)^5$ , it does not reduce the order of the applied numerical method, in other

words, its influence is decreased by the increase of the used resolution. The numerical methods and the actual numerical code we use for calculating time evolution in this paper are also based on those developed in [20,21].

A few nonphysical grid points are introduced for both negative radii  $R < 0$  and for the region ‘‘beyond infinity’’  $R > 1$ . Instead of calculating the time evolution of the  $R < 0$  points, the symmetry property of  $\phi$  about the origin  $R = 0$  is used to set the function values at each time step. Similarly,  $\phi$ , being a massive field, decays exponentially towards infinity, consequently all the field values  $\hat{\phi}$ ,  $\hat{\phi}_t$ , and  $\hat{\phi}_R$  are set to zero for  $R \geq 1$  during the entire evolution. This takes care of the spacelike infinity  $\Omega = 0$  in Eq. (11). Therefore it is possible to use symmetric stencils exclusively when calculating spatial derivatives. The grid point at the origin  $R = 0$  needs special treatment since the last term as it stands on the right-hand side of Eq. (11) is apparently singular. However, this term, when evaluated in terms of the original (nonsingular) field value  $\phi$ , has zero limit value at  $R = 0$ .

Although compactifying in spatial direction restricts the coordinate  $R$  to a finite domain, grid points in our numerical representation get separated by larger and larger physical distances as we approach  $R = 1$ . This far region, where shells of outgoing radiation cannot be represented properly, moves out to higher and higher physical radii as  $\Delta R$  decreases. Numerical simulations with an increasing number of grid points demonstrate that wave packets of outgoing massive fields get absorbed in the transitional region without getting reflected back into the inner domain. In this way our numerical simulations still give a good description of the field behavior precisely in the central region for very long time periods. The simple but physically nonuniform grid together with the help of the dissipation term appears to absorb outgoing radiation in a similar way to the explicit adiabatic dumping term method applied by Gleiser and Sornborger [25]. Furthermore, because of the very low inward coordinate velocity of light in the asymptotic region  $R \approx 1$ , the field behavior in the central region is correctly given for a long time period even after the appearance of numerical errors at  $R \approx 1$ .

Simulating time evolution of oscillons up to their typical maximal lifetime of  $t = 7000$  (measured in Minkowski time units) using spatial resolution of  $2^{13}$  points took usually a week on personal computers. However, because of the need of several runs when fine-tuning parameters in the initial data, we mostly used typical resolutions of  $2^{12}$  spatial points. The parameter  $\kappa$  in the coordinate transformation (8) was set to  $\kappa = 0.05$  in our simulations in order to concentrate approximately the same number of grid points to the central oscillon region and to the far away region where the massive fields form high frequency expanding shells. A Courant factor of  $\frac{\Delta t}{\Delta R} = 1$  turned out to be appropriate to obtain stable simulations with our choice of  $\kappa$ .

The convergence tests confirmed that our code does provide a fourth order representation of the selected evolution equations. Moreover, we monitored the energy conservation and the preservation of the constraint equation  $\partial_R \hat{\phi} = \hat{\phi}_R$ . Most importantly, we compared the field values which can be deduced by making use of the Green's function and by the adaptation of our particular numerical code to the case of massive linear Klein-Gordon fields [26]. The coincidence between the values in the central region provided by these two independent methods for long time evolutions ( $t \approx 10^4$  measured in mass units) made it apparent that the phenomena described below should be considered as true physical properties of the investigated nonlinear field configurations.

### C. Oscillons

Following Refs. [9,17], we start with the following Gaussian-type initial data:

$$\phi|_{t=0} = \phi_\infty + (\phi_c - \phi_\infty) \exp(-r^2/r_0^2), \quad \partial_t \phi|_{t=0} = 0, \quad (12)$$

with  $\phi_c$  and  $\phi_\infty$  being the field values at the center  $r = 0$  and at infinity  $r = \infty$  while  $r_0$  is the characteristic size of the bubble at which the field values interpolates between  $\phi_c$  and  $\phi_\infty$ . By fixing  $\phi_\infty = -1$  as in [9,17] but varying  $r_0$  and  $\phi_c$ , Eq. (12) provides a two-parameter family of smooth and suitably localized initial data. For a large open subset of the possible initial parameters  $\phi_c$  and  $r_0$ , after a short transitional period the field evolves into a long-living localized nearly periodic state, named *oscillon* by Gleiser [8]. Although these configurations live much longer than the dynamical time scale expected from the linearized version of the problem (i.e. light crossing time), their lifetime is clearly not infinite. The energy of these oscillating states is slowly but definitely decreasing in time, and after a certain time period they quickly disintegrate. For the time dependence of the energy in a compact region, see Fig. 3 of [9]. We illustrate in Fig. 1 two such oscillon states with rather different lifetimes.

The parameter dependence of the lifetime is illustrated in Figs. 6, 7, and 8 of [9]. We note that since the final decaying period is relatively short, furthermore its time dependence is almost the same for each particular choice of initial data, the lifetime plots are quite insensitive of the precise definition of how one measures the lifetime of a given configuration. In our calculations the lifetime  $\tau$  was defined by observing when the value of the oscillating field at the center  $r = 0$  falls (and remains) below a certain prescribed value (e.g.  $\phi = -0.95$ ).

Already Copeland, Gleiser, and Müller have noticed that a delicate fine structure appears in the lifetime plot. This peculiar dependence on the precise value of the initial parameter  $r_0$  has motivated the detailed investigation of Honda and Choptuik (see Figs. 4 and 5 of Ref. [17]). The calculations have shown that fixing the value  $\phi_c$  the life-

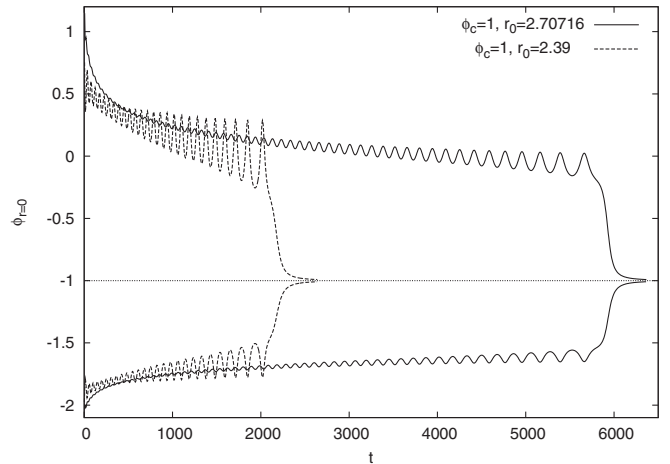


FIG. 1. The upper and lower envelope of the oscillations of the field  $\phi(r = 0)$  is shown for the evolution of Gaussian initial data of the type (12) with two different sets of initial parameters. It is important to note that the field  $\phi$  oscillates with a nonconstant period  $4.6 < T < 5$ . For generic oscillons the period  $T$  shows a decreasing tendency towards  $T \approx 4.6$ .

time increases without any apparent upper limit when the parameter  $r_0$  approaches some element of a large set of discrete resonance values  $r_i^*$ . For example, in the case  $\phi_c = 1$ , Honda and Choptuik have found 125 peaks on the lifetime plot between  $2 < r_0 < 5$ . These fine-tuned oscillons at a later stage during their evolution develop into a state which is very close to a periodic (nonradiating) one. In Fig. 2 we show the field value at the center for typical oscillons close to a chosen peak. The seemingly stable almost periodic stages of the fine-tuned oscillon configurations will be referred as *near-periodic states*. The closer the initial parameters are to the critical value, the longer the lifetime of the near-periodic state becomes. Although the period  $T$  of the underlying high frequency oscillations remains constant to a very good approximation during a chosen near-periodic state, different near-periodic states, corresponding to various peaks on the lifetime curve, oscillate with clearly distinct periods in the range  $4.446 < T < 4.556$ . Generic oscillon states and even the not near-periodic initial part of fine-tuned oscillons pulsate with longer period, in the range  $4.6 < T < 5$ .

Generic oscillons with initial data between two neighboring resonance values  $r_i^* < r_0 < r_{i+1}^*$  may have already quite a long lifetime without developing into a near-periodic state. Plotting the field value at the center  $r = 0$ , one can see a low frequency modulation of the amplitude (called shape mode by Honda and Choptuik) of the high frequency basic oscillating mode (see upper plot of Fig. 2). Oscillons between the next two resonance values  $r_{i+1}^* < r_0 < r_{i+2}^*$  are distinguished from those in the previous interval by the fact that they possess exactly one more or one less peak associated with these low frequency oscillations on the envelope of the field value  $\phi(t, 0)$  before they disperse. Longer living *supercritical* states arise when one

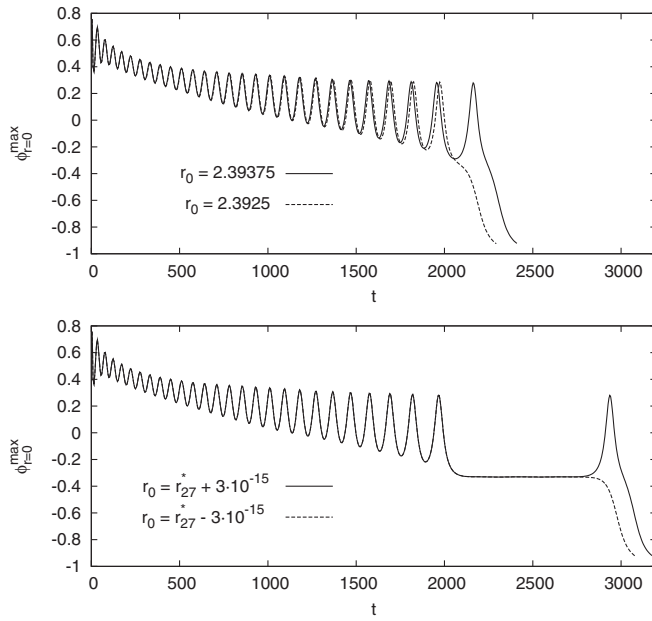


FIG. 2. Upper envelope of the field value for different oscillon states close to the 27th peak of the lifetime curve belonging to  $\phi_c = 1$ . These states are characterized by initial value  $r_0$  which is near  $r_{27}^* \approx 2.39297$ . The *near-periodic state* is approximately at  $2100 < t < 2800$  for the fine-tuned oscillons in the lower plot.

closely approaches a critical value from one of the possible two directions. Then the last low frequency modulation peak gets shifted out to a later and later time as one goes towards the resonance, making room for a near-periodic state between the last two modulations. Close to the resonance, but on the other side of it, the same long-living near-periodic state appears, now called *subcritical*, with the only difference that at the end the field disperses without forming a last low frequency modulation peak.

#### D. Results

It was shown in Ref. [17] that close to a resonance the oscillon lifetime  $\tau$  obeys a scaling law

$$\tau \sim \gamma \ln|r_0 - r_0^*| + \delta, \quad (13)$$

where the scaling exponent  $\gamma$  has specific values for each resonance, while the constant  $\delta$  is also different for subcritical and supercritical states. Although the lifetime appears to increase without any limit by fine-tuning the initial parameter, in practice it is very difficult to achieve very long lifetimes because one cannot represent numbers very close to the resonance value due to the limitation implied by the applied machine precision. Achieving longer lifetime for the near-periodic state is possible by using high precision arithmetics, although then there is a considerable increase of the computation time which limits the applicability of this approach. Using “long double” variables on an appropriate machine, or applying the software “double-double” [27] on a personal computer, we could calculate

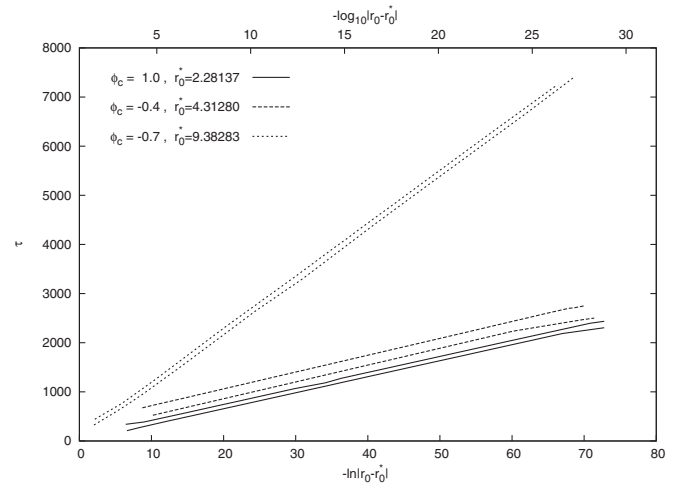


FIG. 3. The oscillon lifetime,  $\tau$ , versus  $-\ln|r_0 - r_0^*|$  is shown for states close to 3 different resonances. The lower lines plotted with a given line type represent subcritical,  $r_0 < r_0^*$ , states while the upper lines with the same line type correspond to supercritical,  $r_0 > r_0^*$ , solutions.

with twice as many significant digits than standard double precision computer variables can represent (i.e. 32 instead of 16). This way we could improve the fine-tuning and double the observed lifetime of near-periodic states. In Fig. 3 we plot the scaling law of the lifetime for oscillons near three different resonances. Instead of choosing three resonances with  $\phi_c = 1$ , we calculated states close to the *first peak* on the lifetime curves corresponding to three different values of  $\phi_c$ . The reason for this was that the normal, slowly but evidently decaying, oscillon state is the shortest near the first peak (i.e. no modulation on the contour curve), thereby we could concentrate computational resources on the near-periodic state.

In order to clarify what we mean by fine-tuning the parameter  $r_0$  to 16 (or 32) digits and what is the actual error of the quantities, we present a table (Table I) on the precise location of the first peak for  $\phi_c = 1$  when performing fine-tuning with five different numerical resolutions. For each spatial resolution we could achieve approximately the same lifetime of approximately  $\tau = 1100$

TABLE I. The position  $r_0^{*(i)}$  of the first peak for  $\phi_c = 1$  using various resolutions. The number of spatial grid points used for a specific fine-tuning is  $n_i = 2^i$ . The error is estimated as  $\delta_i = |r_0^{*(i)} - r_0^{*(12)}|$ . The convergence factor is defined as  $c_i = \log_2|(r_0^{*(i-2)} - r_0^{*(i-1)}) / (r_0^{*(i-1)} - r_0^{*(i)})|$ .

$i$	$n_i$	$r_0^{*(i)}$	$\delta_i$	$c_i$
8	$2^8$	2.281 990 488 596 033	$6.210^{-4}$	
9	$2^9$	2.281 392 051 715 203	$2.110^{-5}$	
10	$2^{10}$	2.281 371 382 459 355	$7.910^{-7}$	4.86
11	$2^{11}$	2.281 370 625 452 998	$3.110^{-8}$	4.77
12	$2^{12}$	2.281 370 594 875 569		4.63

when the parameter  $r_0$  approximated a resolution dependent value to 16 digits. The convergence of the data indicates that the actual position of the peak is at  $r_0^* = 2.281\,370\,594$  with an error of  $10^{-9}$ .

Our numerical simulations clearly show that the different resonance peaks on the lifetime plot correspond to different near-periodic states. In fact, a one-parameter family of distinct near-periodic states appears to exist. This statement is in marked contrast with the claim of Honda and Choptuik in [17], where in Sec. III A they claim that the oscillation period is almost the same for all oscillons and is roughly  $T \approx 4.6$ , which corresponds to a pulsation frequency of  $\omega \approx 1.366$ . From our numerical analysis, we can clearly see that the period of the oscillation depends on the resonance considered. In Fig. 4 the upper envelope of the oscillating field value at the origin is shown as a function of time for oscillon states close to the same three resonances as in Fig. 3. In Fig. 5 the time dependence of the frequency at the origin is shown for the same three states during the time period where the oscillation is almost periodic (i.e. during the near-periodic states). The frequency  $\omega$  of the oscillations along with its time dependence at some radius  $r = \bar{r}$  has been determined from our numerical results by minimizing the following integral for the oscillation period  $T = 2\pi/\omega$ :

$$\int_{t-t_0}^{t+t_0} [\phi(t, \bar{r}) - \phi(t + T, \bar{r})]^2 dt \quad (14)$$

using some suitably chosen integration interval determined by  $t_0$ . This procedure, applying polynomial interpolation, yields significantly more precise frequency values than the direct use of the fast Fourier transform method, especially when the time step by which our evolution code outputs data is not extremely short. Another advantage of our procedure is it being much less sensitive to the particular

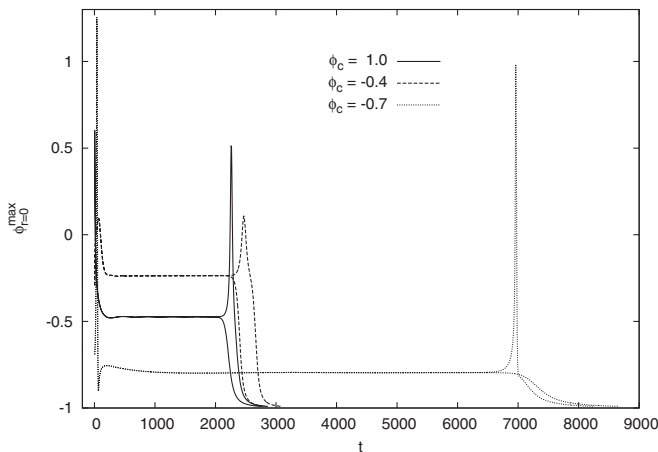


FIG. 4. Upper envelopes of the oscillations of the field value at  $r = 0$  for three pairs of subcritical and supercritical oscillon states close to the first resonances corresponding to three given  $\phi_c$  initial parameters. The fine-tuning was performed using 32 digit arithmetics.

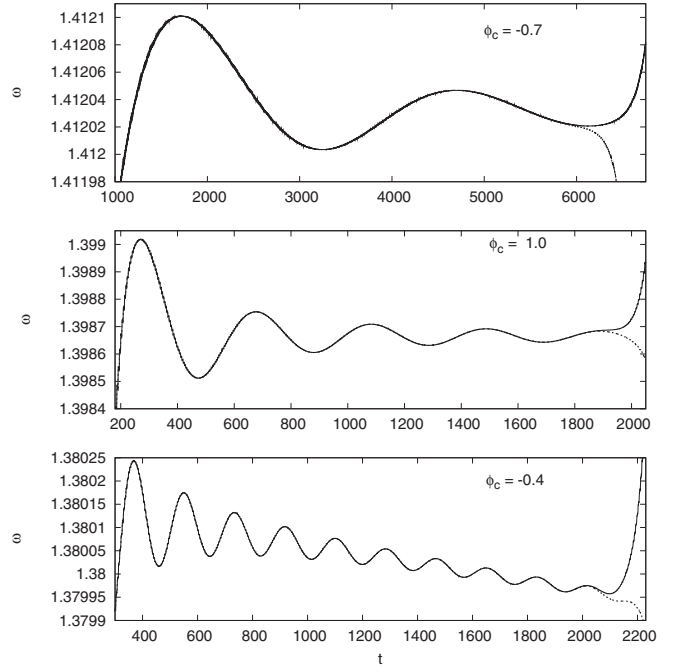


FIG. 5. The pulsation frequency,  $\omega$ , in function of the time for the three pairs of oscillons shown on the previous figure during their corresponding near-periodic states.

choice of the sampling interval (in this case  $2t_0$ ) than the fast Fourier transform algorithm. The relatively small value of  $t_0$  (for example  $t_0 = 10$ ) makes it possible to monitor relatively sharp changes in the time dependence of the frequency.

All three near-periodic states show a low frequency change of  $\omega$  with a decaying amplitude, with the lowest frequency modulation belonging to the state with the highest  $\omega$ . The amplitudes in Fig. 4 would show a similarly decaying slight modulation if we would plot them individually in time intervals where the oscillations are almost time periodic. These observations suggest that near-periodic states of frequency  $\omega$  also contain a superposition of states with frequencies  $\omega \pm \Delta_\omega$  where  $\Delta_\omega/\omega \ll 1$ . In the next sections we shall see that at least the core part of an oscillon of frequency  $\omega$  can be extremely well described by a weakly localized quasibreather of the same frequency.

We emphasize that the three chosen near-periodic states are typical, i.e. the near-periodic states of all fine-tuned oscillons (including all peaks belonging to  $\phi_c = 1$ ) are qualitatively and quantitatively very similar to them. Actually, the frequency of all calculated near-periodic states fell into the interval  $[1.379, 1.413]$  spanned by the frequency of the two chosen first peaks belonging to  $\phi_c = -0.4$  and  $\phi_c = -0.7$ .

On the third plot of Fig. 5, we can also see a slow but steady decrease of the frequency  $\omega$ . For the other two states, with frequencies closer to  $\sqrt{2}$  no such behavior is apparent in the time interval we could simulate. This slow

decrease is also manifested in the energy of the configuration. In Fig. 6 we plot the time dependence of the energy contained inside spheres with three subsequent radii. The decrease of the energy indicates that the near-periodic state slowly loses its energy, consequently it cannot be exactly time periodic. Looking at the energy in the sphere at  $r = 40.1$ , we can see that the decrease of energy from  $t = 1000$  to  $t = 2000$  is  $\Delta E = 0.0041$ . Taking into account that the total energy is  $E = 21.60$ , we can give a naive estimate on the lifetime by calculating when the energy would decrease into its half value at this rate, getting  $\tau_e = 2.6 \times 10^6$ . We expect that all near-periodic states radiate, but this radiation is becoming considerably weaker as the frequency gets closer to  $\sqrt{2}$ . This expectation is confirmed by the direct analysis of periodic solutions in the next sections.

In Fig. 6 the curve corresponding to the largest radius ( $r = 107.1$ ) indicates how slowly the energy moves outwards because of the massive character of the field. The different endings of the curves belonging to subcritical and supercritical states illustrate the two kinds of decay mechanism of near-periodic states. In the first, subcritical mechanism, the field quickly disperses, while energy moves essentially outwards only. In the second supercritical way, the energy of the field first collapses to a smaller region near the origin and then disperses to infinity. This resembles the behavior of some unstable spherical shell, although no shell structure is visible on the density plots, being the highest energy density always at the center. The instability of the near-periodic states with two distinct kinds of decay mechanisms gives a qualitative explanation on why it is possible to reach long lifetimes by fine-tuning the initial parameters.

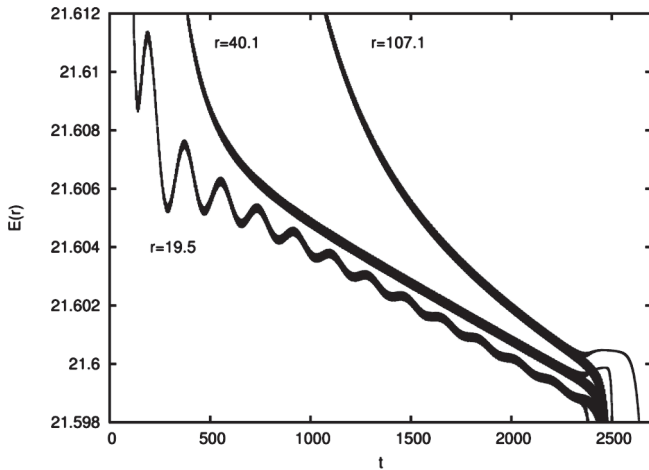


FIG. 6. The time dependence of the energy contained in spheres of radii  $r = 19.5$ ,  $r = 40.1$ , and  $r = 107.1$  for the  $\phi_c = -0.4$  first peak. The thickness of the curve indicates that the high frequency oscillation is still not negligible at these high radii. The different endings of the curves correspond to subcritical and supercritical states.

### E. Fourier decomposition of the evolution results

Since during the time evolution the field  $\phi$  becomes approximately time periodic for any longer living oscillon state, it is natural to look at the Fourier decomposition of the results provided by our evolution code. Since the fast Fourier transform algorithm is very sensitive to the size of the time step with which our evolution code writes out data, we use an alternative direct method which turns out to be significantly more precise in determining the basis frequency and the amplitude of the higher modes. As a first step, we determine the oscillation period by locating two subsequent maxima, at instants  $t_1$  and  $t_2$ , of the field at the origin  $r = 0$ . Since  $t_1$  and  $t_2$  fall in general between two consequent time slices written out by our evolution code, we approximate their position by fitting second order polynomials on the data. It is apparent from our results that for near-periodic states these maxima correspond to two consecutive moments of time symmetry not only at the center but also in a large region around the center to a very good approximation. After determining the oscillation frequency  $\omega = 2\pi/(t_2 - t_1)$ , we obtain the  $n$ th Fourier mode at a radius  $r$  by calculating the following integral using the output  $\phi(t, r)$  of the evolution code

$$\phi_n(r) = \int_{t_1}^{t_2} (\phi(t, r) + 1) \exp(in\omega t) dt. \quad (15)$$

We note that care must be taken for the first and last incomplete time steps when evaluating the integral (15). In the case of exact periodicity and time symmetry, the imaginary part of this integral would be zero for all  $n$ . In order to check the deviation from time symmetry for various radii at the moments  $t_1$  and  $t_2$ , we also evaluate the imaginary part of the integral for each  $n$  and verify whether it is small compared to the real part.

As an example, in Fig. 7 we give the Fourier decomposition of the  $\phi_c = -0.7$ ,  $r_0 = 9.38283$  near-periodic

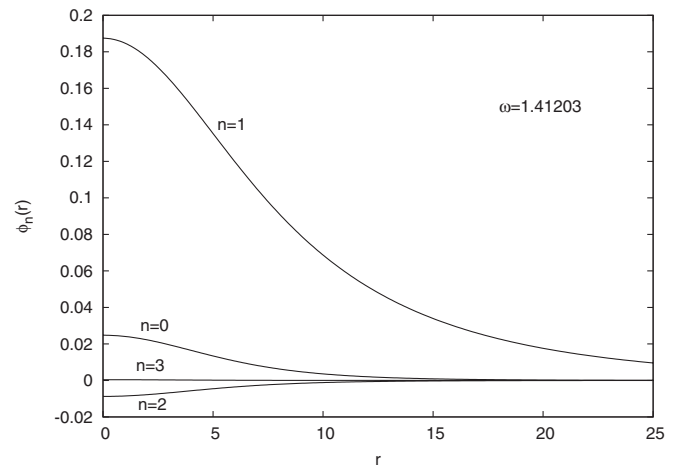


FIG. 7. Radial dependence of Fourier modes obtained by decomposition of a near-periodic state with frequency  $\omega = 1.41203$ .

state presented in Fig. 5. The integral (15) was calculated between two subsequent maximums of the field at the center at  $t_1 = 5420.22$  and  $t_2 = 5424.67$ , yielding an oscillation frequency of  $\omega = 1.41203$ . For the decomposition of a near-periodic state with a lower frequency see Fig. 9 of [17], where the frequency is  $\omega = 1.38$  (page 107 of [18]). From the two plots, one can already see the general tendencies. As the basis frequency increases towards the upper limit  $\sqrt{2}$  the oscillon becomes wider, although with a decreasing amplitude. The influence of the higher modes (the relative amplitude ratio) is also getting smaller when the frequency grows.

### III. FOURIER DECOMPOSITION OF THE QUASIBREATHERS

This section is concerned with a direct search for time-periodic solutions of the NLWE Eq. (3) by means of a Fourier-mode decomposition of the scalar field  $\phi$ . A simple parameter counting already indicates that an infinite number of parameters would be necessary in order to obtain an exponentially localized breather, so even if some do exist, it seems to be difficult to produce them directly. Therefore we look for weakly localized solutions of Eq. (3), and by analyzing their behavior in the function of the free parameters we expect to obtain a clear indication about the existence of truly localized breathers.

#### A. Equations and their asymptotic behaviors

Since we seek periodic solutions of Eqs. (3), we make a Fourier-mode decomposition of the form

$$\phi(t, r) = -1 + \tilde{\phi} = -1 + \phi_0(r) + \sum_{n=1}^{\infty} \phi_n(r) \cos(n\omega t). \quad (16)$$

We have assumed here that by a suitable choice of the time origin the solutions are time symmetric. Inserting this form in Eq. (3) gives rise to a system of coupled elliptic equations

$$\begin{aligned} [\Delta - 2]\phi_0 &= \phi_0^2(\phi_0 - 3) + \frac{3}{2}(\phi_0 - 1) \sum_{m=1}^{\infty} \phi_m^2 \\ &+ \frac{1}{4} \sum_{m,p,q=1}^{\infty} \phi_m \phi_p \phi_q \delta_{m,\pm p \pm q} \\ [\Delta - \lambda_n^2]\phi_n &= 3\phi_0(\phi_0 - 2)\phi_n \\ &+ \frac{3}{2}(\phi_0 - 1) \sum_{m,p=1}^{\infty} \phi_m \phi_p \delta_{n,\pm m \pm p} \\ &+ \frac{1}{4} \sum_{m,p,q=1}^{\infty} \phi_m \phi_p \phi_q \delta_{n,\pm m \pm p \pm q}, \end{aligned} \quad (17)$$

where  $\lambda_n^2 = (2 - n^2\omega^2)$ . In fact we have already regrouped together all the linear (first order) terms of the corresponding Fourier mode,  $\phi_n$ , to the left-hand side of Eqs. (17). We will make a systematic search for localized solutions of the system (17). We shall not assume any *a priori* connection with the oscillons presented in the previous section for the possible frequencies,  $\omega$ . As we shall see below, the eventual existence of a localized solution can only be possible if system (17) exhibits some very special properties.

In order to look for regular solutions of Eqs. (17), we analyze the various asymptotic behaviors of the homogeneous solutions of the corresponding operator on the left-hand side of Eqs. (17).

- (i) If  $\lambda_n^2 > 0$  then there is one regular homogeneous solution, which falls off exponentially:  $\exp[-|\lambda_n|r]/r$ . This function clearly decays sufficiently fast at infinity so that the energy would always be convergent.
- (ii)  $\lambda_n^2 = 0$  is a degenerate case when the operator is the usual Laplacian. The nonsingular (decaying) homogeneous solution is simply  $1/r$  which, however, does not decay sufficiently fast for the energy to be bounded.
- (iii) If  $\lambda_n^2 < 0$ , both homogeneous solutions tend to zero at infinity,  $\cos[|\lambda_n|r]/r$  and  $\sin[|\lambda_n|r]/r$ . As for the previous case, these functions do not decrease fast enough to make the energy convergent. Apart from that, both functions are regular at infinity and this implies that there is no uniqueness of the solution which is only defined up to a given phase (for more details, see Sec. IV C).

Observe that no matter what the value of  $\omega$  is, there always exists an  $n_\omega$ , such that *all modes*,  $\phi_n, n > n_\omega$  will be of the third type (i.e. with  $\lambda_n^2 < 0$ ). It is now easy to understand why, in the generic case, one cannot expect to find exponentially localized (with finite energy) solutions of Eqs. (17). To ensure localization, one has to suppress all slowly decaying oscillatory modes which would normally require an infinite set of freely tunable parameters. The problem of finding a localized solution can be seen as a matching problem between the set of modes regular in a neighborhood of the origin,  $\{\phi_n^0\}_{n=0}^{\infty}$ , and the set of modes with fast (exponential) decay for  $r \rightarrow \infty$ ,  $\{\phi_n^\infty\}_{n=0}^{\infty}$ . In this case each mode  $\phi_n^0$ , regular at the origin, has a single freely tunable parameter, whereas none of the modes with fast falloff,  $\phi_n^\infty$  for  $n > n_\omega$ , have any free parameters and therefore a sort of a miracle is needed that the two sets could be matched. This counting implies that while one can expect to find time-periodic solutions Eqs. (17) (even a whole family), these solutions have generically oscillatory tails for large values of  $r$ . This clearly reflects the argument “*anything that can radiate does radiate*” transposed to the stationary case. On the other hand, it is not excluded that a localized solution might exist for very particular values of  $\omega$ , for which the oscillatory tails are absent.

## IV. NUMERICS FOR THE MODE DECOMPOSITION

### A. Partial differential equation solver

We solve the system (17) using the LORENE library [28]. The basic features of LORENE are the use of spectral methods and multidomain decomposition. The problem we are facing here being purely spherical, the fields are expanded on Chebyshev polynomials. The physical space is decomposed in various spherical domains.

Using such techniques, solving differential equations can be reduced to, in each domain, inverting a matrix on the coefficients space. Then, a linear combination of the particular solutions with the homogeneous ones is done, in order to impose regularity at the origin, appropriate boundary conditions, and continuity of the overall solution. We refer the reader to [29] for more details on the algorithm, in the case of a Poisson equation.

For this work, we have extended the operators presented in [29] and included the Helmholtz operators appearing in Eqs. (17), i.e.  $\Delta - \lambda_n^2$  with both signs of  $\lambda_n^2$ . This is rather straightforward because, as for the Laplacian, they produce two homogeneous solutions. Only the case of infinity has to be treated differently as we will see in Sec. IV C.

### B. Description of the sources

As we have seen in Sec. III A, for all value of  $\omega$ , there exists a value of  $n$  after which all the modes are dominated by homogeneous solutions of the type  $\sin(|\lambda_n|r + \varphi_n)/r$ . Such functions are not easily dealt with by our solver. Indeed, in order to treat spatial infinity, LORENE usually uses a simple compactification by means of the variable  $u = 1/r$  in the exterior domain. In the past, this has enabled us to impose exact boundary conditions at infinity. When waves are present, it is well known [30,31] that such a compactification is not practical. Indeed, no matter what scheme is used, there is always a point after which the distance between computational points (grid or collocation) is greater than the characteristic length of change of the wave, thus causing the scheme to fail. This issue is dealt with by imposing boundary conditions at a finite radius  $R_{\text{lim}}$  for the slowly decaying oscillatory modes. The reader should refer to [32] where such methods have been applied to gravitational waves. For the exponentially decaying modes in Eqs. (17), we decide to keep in the right-hand side (in the sources) only those terms that are dominated by the exponentially decaying homogeneous solutions, i.e., only those modes for which  $\lambda_n^2 > 0$ . As it will be seen later, the range of interesting pulsations is  $\omega < \sqrt{2}$ . Therefore the only two exponentially decaying modes are  $\phi_0$  and  $\phi_1$ . In the equations for  $\phi_0$  and  $\phi_1$  for  $r > R_{\text{lim}}$ , we set all the higher modes ( $n \geq 2$ ) to zero (including terms of the type  $\phi_3 \phi_1^2$ ). So, we effectively solve for large values of the radius the following equations:

$$[\Delta - 2]\phi_0 = \frac{3}{2}(\phi_0 - 1)\phi_1^2 + \phi_0^2(\phi_0 - 3) \quad (18)$$

$$[\Delta - \lambda_1^2]\phi_1 = 3\phi_0(\phi_0 - 2)\phi_1 + \frac{3}{4}\phi_1^3. \quad (19)$$

This method yields solutions for  $\phi_0$  and  $\phi_1$  which are correct for “intermediately large” values of  $r > R_{\text{lim}}$ , where the oscillatory and slowly decaying terms induced by the nonlinearities do not dominate. It is clear that for sufficiently large values of  $r$ ,  $\phi_0$  and  $\phi_1$  do not decay exponentially, since their behavior will be dominated by the slowly decaying oscillatory nonlinear source terms. We have carefully checked that changing the value of  $R_{\text{lim}}$  does not influence the oscillatory modes, therefore we can conclude that the backreaction of the  $\phi_0$  and  $\phi_1$  is negligible on  $\phi_n$ ,  $n \geq 2$  for  $r \gg R_{\text{lim}}$ .

### C. The operators

When  $\lambda_n^2 > 0$ , the Helmholtz operator  $\Delta - \lambda_n^2$  admits two homogeneous solutions of which only one tends to zero at infinity. This situation is exactly the same as the one for the standard Laplace operator and all the techniques presented in [29] can be used. Once again, as we will be working for  $\omega < \sqrt{2}$ , this happens only for  $\phi_0$  and  $\phi_1$  and the associated sources have been given in the previous Sec. IV B.

The situation is quite different when dealing with the Helmholtz operator with  $\lambda_n^2 < 0$ . Apart from the compactification problem previously mentioned, we have to note that now there are two homogeneous solutions that are regular at infinity. There is no reason to prefer one to the other. This means that there is no unique solution to our problem. Indeed, one can get a solution by doing the matching with any homogeneous solution of the type  $\sin(|\lambda_n|r + \varphi_n)/r$ , where  $\varphi_n$  can take any value in  $[0, 2\pi[$ . So to summarize, for all modes such that  $\lambda_n^2 < 0$  we have to match, at a finite radius  $R_{\text{lim}}$ , the solution with a homogeneous one of the type

$$\phi_{n \geq 2}(r > R_{\text{lim}}) = A_n \sin(|\lambda_n|r + \varphi_n)/r. \quad (20)$$

Clearly, we need additional conditions to fix the values of the phases  $\varphi_n$ . In order to do so, let us recall that we are mainly interested in finite energy solutions. Such solutions should not contain any oscillatory behavior in  $1/r$  at infinity, i.e. *all* the coefficients  $A_n$  of such homogeneous solutions should be zero. One can hope to achieve that by searching, in the parameter space of the phases  $(\varphi_2, \dots, \varphi_n)$ , the values that minimize the absolute value of the coefficient of the first oscillatory homogeneous solution that appears:  $|A_2|$ . This solution being “quite close” to a localized breather, for that reason we refer to it as a quasibreather.

Given the nonlinearity of the problem, the location of the minimum cannot be found analytically and one has to rely on a numerical search. We make use of the multidimensional minimizer provided by the GSL numerical library

[33]. The algorithm is based on the simplex algorithm of Nelder and Mead [34]. We start by setting all the phases to  $\pi/2$  and iterate the procedure until the value of the minimum converges with a given threshold. Let us mention that the phases are searched in  $[0, \pi[$ , the rest of the interval, being described by changing the sign of the amplitudes. The simplex solver converges rapidly, the function  $|A_2|$  being very smooth, with no local extrema.

So the final situation is the following:

- (i) For  $\phi_0$  and  $\phi_1$  the space is compactified and the sources in the exterior region are given by Eqs. (18) and (19).
- (ii) For  $\phi_n, n \geq 2$ , we only solve for  $r < R_{\text{lim}}$  and match the solution with a homogeneous solution  $A_n \sin(|\lambda_n|r + \varphi_n)/r$ , the  $\varphi_n$  being determined by the simplex solver by minimizing  $|A_2|$ .

#### D. Avoiding the trivial solution

The system (17) is solved by iteration but a problem arises from the fact that the trivial solution  $\phi_n = 0$  is a solution of the equations (then  $\phi_0$  is a constant whose value is either 0, 1, or 2). No matter what the initial guess for the different modes is, the code always converges to a trivial static solution of this type.

So, one needs to find a way to prevent this from happening. Given that the system (17) is coupled, it is sufficient to impose  $\phi_1(r=0) \neq 0$ , in order to avoid the trivial solution. To do so, after each step of the iteration, we rescale  $\phi_1$  everywhere, by a factor  $\alpha$  in order to impose that  $\phi_1(r=0)$  has a certain value. In the general case, after convergence of the code, this scaling parameter is different from 1 meaning that the value of  $\phi_1$  we found is no longer the solution of the system (17). However, for some values of  $\omega$  (being in an interval, see Sec. V), it is possible to find exactly one value of  $\phi_1(r=0)$  such that the scaling factor is one. Thus, it is possible, at least for some values of  $\omega$ , to find the appropriate value of  $\phi_1(r=0)$  such that the obtained modes are nontrivial solutions of Eqs. (17).

In practice, after convergence to a threshold level of typically  $10^{-3}$ , we switch on the convergence toward the true value of  $\phi_1(r=0)$ . With a technique already used, for example, to get neutron stars of appropriate mass (see Sec. IV D 3 of [35]), at each step, we change the value of  $\phi_1$  at the center, in order to make  $\alpha$  closer to one. The value of  $\phi_1(r=0)$  to which one wants to converge is modified according to

$$\phi_1(r=0) \rightarrow \phi_1(r=0) \left[ \frac{2 - \log \alpha}{2 - 2 \log \alpha} \right]^{0.1}. \quad (21)$$

Doing so, the value of  $\phi_1$  at the center converges to the only value such that the scaling parameter  $\alpha$  is one, providing us with the real, nontrivial, solution of the system (17).

#### E. Influence of the phases

In order to verify that the simplex solver converges to the proper minimum of  $|A_2|$ , we show in Fig. 8 how various quantities vary when one changes the precision at which the extremum is found. Figure 8 presents the values of:

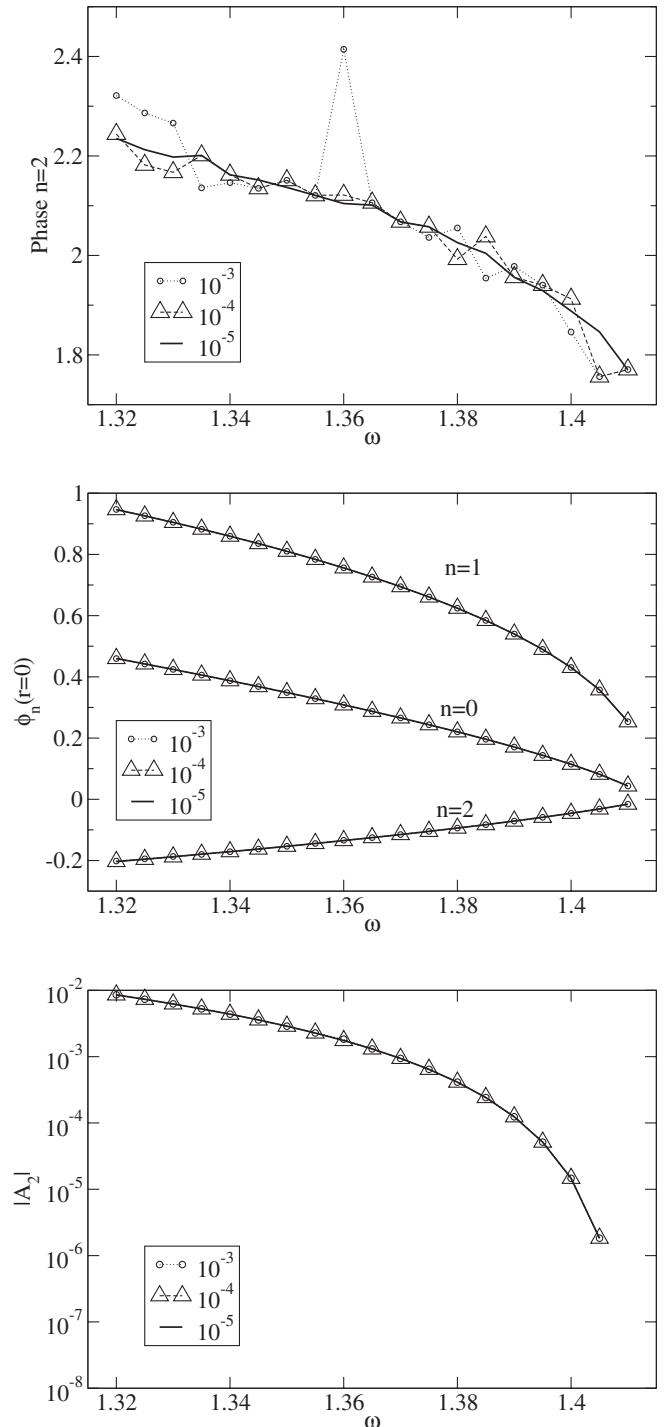


FIG. 8. Convergence of the various results with respect to the precision required when finding the minimum of  $|A_2|$ .

- (i) the phase of the second mode  $\varphi_2$  at which the minimum is found,
- (ii) the values of the first modes at the origin  $\phi_n(r=0)$ ,
- (iii) and the value of the minimum of  $|A_2|$ .

Those three quantities are shown as a function of  $\omega$ , for three different values of the precision required for the simplex solver,  $10^{-3}$ ,  $10^{-4}$ , and  $10^{-5}$ .

From the values of the phase  $\varphi_2$ , it appears that a precision of  $10^{-3}$  or  $10^{-4}$  is not good enough, the curve being quite noisy. The curve obtained with a precision of  $10^{-5}$  is smoother and we will assume that this level of precision is sufficient for the purpose of this paper and this value will be chosen for all the rest of this work. The situation is even better for both the values of the modes at the origin and the actual value of the minimum. Indeed, as can be seen in Fig. 8, those quantities show almost no dependence on the level of precision. This is simply related to the fact that the values of the fields depend very weakly on the values of the phases of the homogeneous solutions in the external region. This is true for the phase of the second mode  $\varphi_2$  but even more for the higher order phases  $\varphi_{n>2}$ .

The very moderate dependence of  $A_2$  on the phases is illustrated by Fig. 9, where the value of the amplitude is shown as a function of the phase  $\varphi_2$  for  $\omega = 1.37$ . All the other phases  $\varphi_{n>2}$  are fixed to the same value, each of them corresponding to one curve in Fig. 9. It is clear that the influence of the phases of the modes  $n > 2$  is very weak. The extrema on the three curves of Fig. 9 are very close to the real extremum found by the simplex solver. Therefore we are quite confident that we can find the minimum of  $|A_2|$  with good accuracy, even if the associated values of the phases are slightly less accurate.

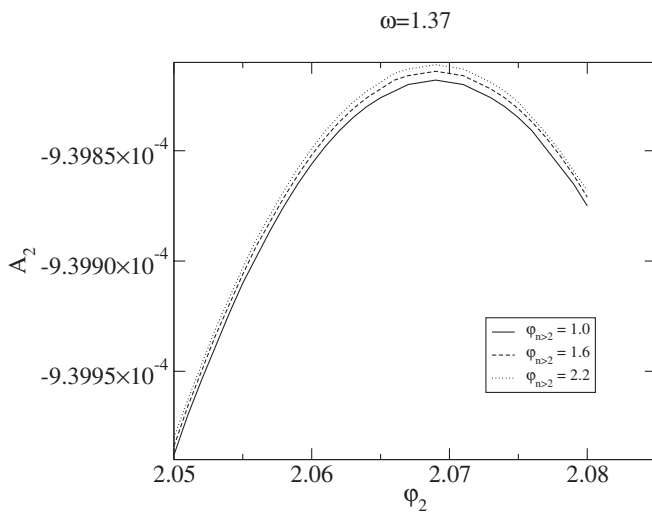


FIG. 9. Value of  $A_2$  as a function of the phase  $\varphi_2$ , for  $\omega = 1.37$ . The other phases are maintained equal and set to 1.0 (solid line), 1.6 (dashed line), and 2.2 (dotted line).

## F. Convergence tests

In order to further check the validity and accuracy of our code with respect to the computational parameters, we present in this section various additional convergence tests. The idea is to take a reference set of computational parameters and to change one of those at a time, in order to check that the obtained results do not change much. The first three radial domains are chosen with boundaries  $[0, 1]$ ,  $[1, 2]$ , and  $[2, 4]$ . After  $r = 4$ , we keep the size of the domain constant to 4 [i.e. the boundaries of the domain  $i$  are  $[4(i-3), 4(i-2)]$ ]. We found that this is necessary to ensure that in every domain we have enough collocation points to resolve the oscillatory homogeneous solutions.

The various computational parameters are the following:  $n_z$  is the number of radial domains which relates directly to the value of  $R_{\text{lim}}$  given the setting of the domain mentioned above.  $N_r$  is the number of coefficients in each domain. Finally, we will also check the convergence of the results with respect to the finite number of modes we consider in the system (17).

Our standard setting consists of  $n_z = 14 \Rightarrow R_{\text{lim}} = 44$ ,  $N_r = 33$ , and the use of 6 modes. We then change one parameter at a time to verify that the obtained results are indeed meaningful. The convergence is presented by showing the same three quantities as in Sec. IV E: the phase  $\varphi_2$ , the values of the first modes at the origin, and the amplitude  $|A_2|$ .

The three plots of Fig. 10 show the dependence of the results when varying the number of coefficients in every domain. Since for the values of  $N_r$  the curves of Fig. 10 change only slightly, this is a strong sign that  $N_r = 33$  is greatly sufficient to get accurate results. It is also supported by the fact that, after the end of the iterative scheme, we find that the relative difference between the right- and left-hand sides of Eqs. (17) is smaller than  $10^{-9}$ .

A strong test is provided by the plots of Fig. 11. They show that the results are independent of the value of the outer computational radius  $R_{\text{lim}}$  thus validating the matching procedure with the oscillatory homogeneous solutions. Finally, Fig. 12 illustrates the fact that the results do not change substantially when increasing the number of modes.

The last test of our code has been a comparison of the right-hand side (rhs) and left-hand side (lhs) of Eq. (3), using the Fourier expansion (16). We have computed the relative difference between the rhs and lhs after averaging over one period. The results for various number of modes are depicted in Fig. 13 as a function of  $\omega$ . As expected, the error decreases as the number of modes increases. This is not surprising, given that Eq. (17) could be satisfied only for an infinite number of modes. The error also increases when  $\omega$  decreases. This can be understood by recalling that the modes are more important when  $\omega$  is small [i.e. see the behavior of  $\phi_n(r=0)$  as a function of  $\omega$  in Figs. 10–12]. Thus, the effect of the missing modes is more important for smaller  $\omega$ .

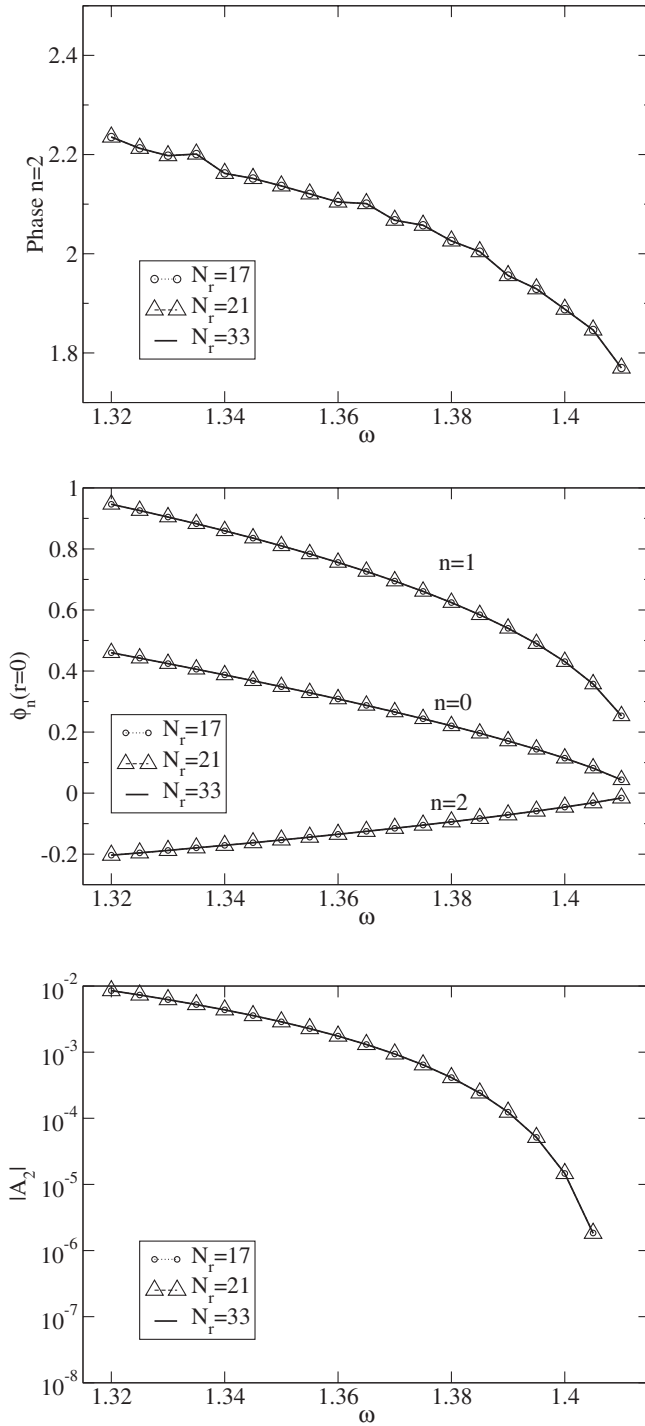


FIG. 10. Same as Fig. 8 but when varying the  $N_r$  in each domain.

Finally, we would like to emphasize that the computational parameters exhibited in this section are sufficient to compute solutions in the regime of "moderate" frequencies (i.e. frequencies around 1.37–1.38). If one wishes to go to much lower frequencies, one would need to include more modes, for higher order modes will be more important, as indicated by Fig. 13. On the other hand, as will be

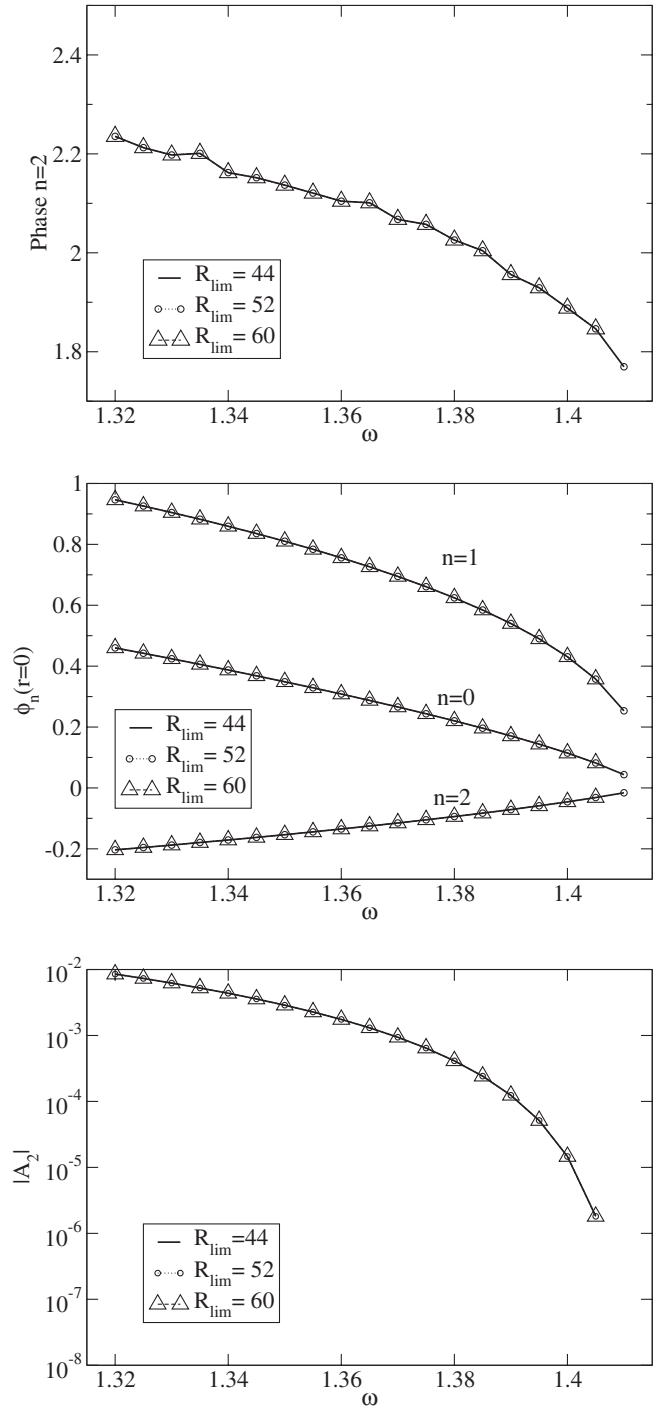


FIG. 11. Same as Fig. 8 but changing the value of  $R_{lim}$ .

seen in the next section, the matching point  $R_{lim}$  must be increased when one approaches the critical value  $\omega_c = \sqrt{2}$ .

## V. RESULTS

As illustrated in Figs. 10–12, we do find time-periodic quasibreather solutions of Eqs. (17) for any value of the pulsation frequency  $1.32 \leq \omega \leq 1.41$ , and there is little

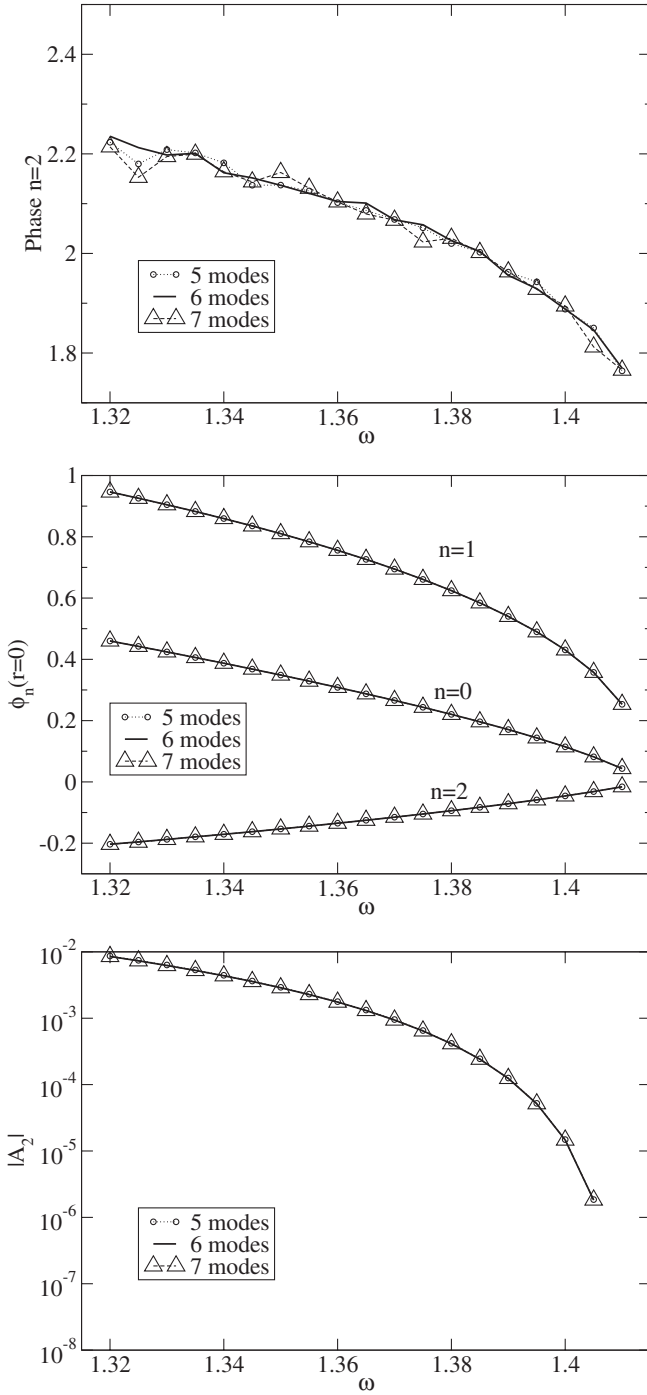


FIG. 12. Same as Fig. 8 but varying the number of modes.

doubt that such solutions exist for all frequencies in the range  $]0, \sqrt{2}[$ . It is also clear from the very same figures that for  $\omega \rightarrow \omega_c = \sqrt{2}$  the family of solutions we consider converges pointwise to the trivial solution. We do not expect such quasibreather solutions of the system (17) to exist for  $\omega > \omega_c$ . The critical value  $\omega_c = \sqrt{2}$  is expected to be related to the change of nature of the Helmholtz operator for  $\phi_1$ ,  $\sqrt{2}$  being the value at which  $\phi_1$  ceases to decay like an exponential. In the 1 + 1 dimensional

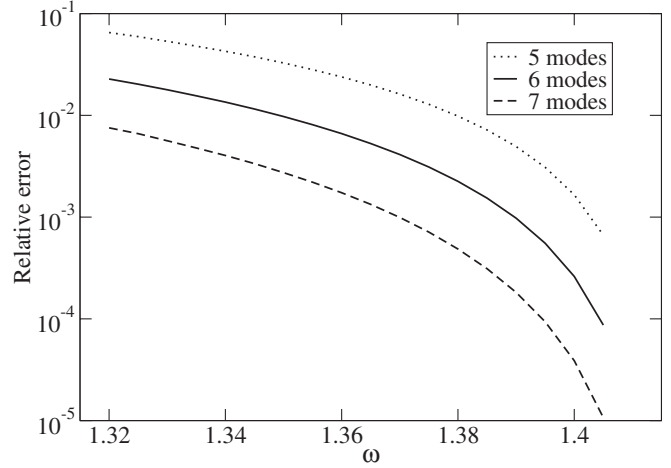


FIG. 13. Relative difference between the lhs and rhs members of Eq. (3). The result is averaged over one period and we present the error as a function of  $\omega$ , for 5, 6, and 7 modes.

case, Coron [36] has proved that the allowed frequencies are indeed constrained by  $\omega < \omega_c$ . We have not attempted to prove the analogous statement for our case, as it would certainly require some sophisticated mathematical tools.

The quasibreather solutions obtained this way are not well localized in space because of their slowly decaying  $\propto 1/r$  oscillatory tail. Consequently, none of these solutions has finite energy. In fact, we have selected a special class of time-periodic solutions by minimizing the amplitude of their oscillatory tail. This is, in some sense, the closest one can get to a breather and we have called those configurations “quasibreaters.” There is no special value of  $\omega$  for which the amplitude of the oscillatory tail would show any tendency to become very small or going to zero. This is illustrated in Fig. 14 where the logarithm of the coefficients of “tails” are shown for the modes  $\phi_2, \phi_3, \phi_4$ , and  $\phi_5$ , as a function of  $\omega$ . The only value of  $\omega$  for which the curves go to zero is the critical one for which the

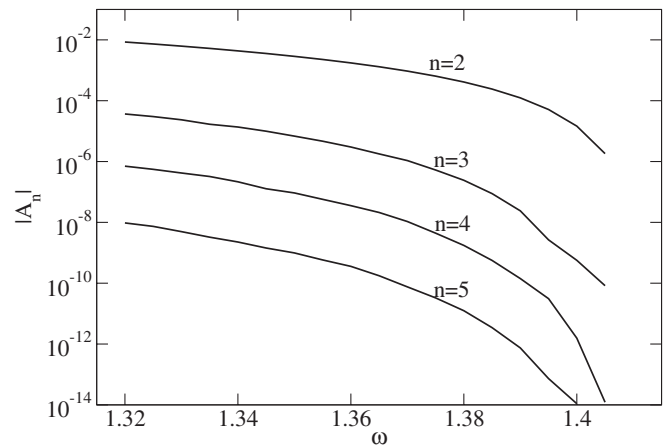


FIG. 14. Coefficients of the oscillatory homogeneous solutions  $\phi_n$  ( $n = 2, 3, 4, 5$ ) as a function of  $\omega$ .

solution tends to the trivial one. The many convergence tests of Sec. IV F show that we can accurately compute the value of those coefficients and that they are not numerical artifacts.

To illustrate the behavior of the quasibreathers, we show in Fig. 15 and 16 the energy density  $\xi$  and the one including the volume element, i.e.  $r^2\xi$  as a function of the radius, for values of  $\omega$  going from 1.36 to 1.40. We can clearly see two qualitatively different behaviors: (i) the solutions have a well defined ‘‘core,’’ where the behavior is dominated by the exponential decay of the fields and so the density goes to zero. This core is getting larger when  $\omega \rightarrow \sqrt{2}$ . (ii) However, inevitably at some point, the oscillatory tails start to dominate and the density reaches a plateau, ultimately causing the total (integrated) energy to be infinite. Let us mention that if for high values of  $\omega$  the plateau is not seen, it comes solely from the fact that the value of  $R_{\text{lim}}$  used in Fig. 15 and 16 is not sufficient. In spite of the numerical smallness of the amplitude of this plateau, we

are quite confident that its value is reasonably accurate, and also that it really corresponds to a physical effect. Indeed, its value is very stable when varying the various computational parameters.

As  $\omega$  increases, the value of the plateau diminishes. This is related to the fact that the coefficients of the homogeneous solutions are decreasing functions of  $\omega$  and to the quadratic nature of the energy density in  $\phi$ , i.e. the value of the plateau is roughly the square of the greatest coefficient (i.e. the one for  $\phi_2$ ).

As already stated, we can also confirm that the transition radius between the core and the plateau increases as one approaches  $\omega = \sqrt{2}$ . To be more quantitative, we define the transition radius  $R_{\text{trans}}$  as the first value of  $r$  for which  $\phi_1$  reaches the amplitude of the oscillations:

$$\phi_1(r = R_{\text{trans}}) = \frac{|A_2|}{r}. \quad (22)$$

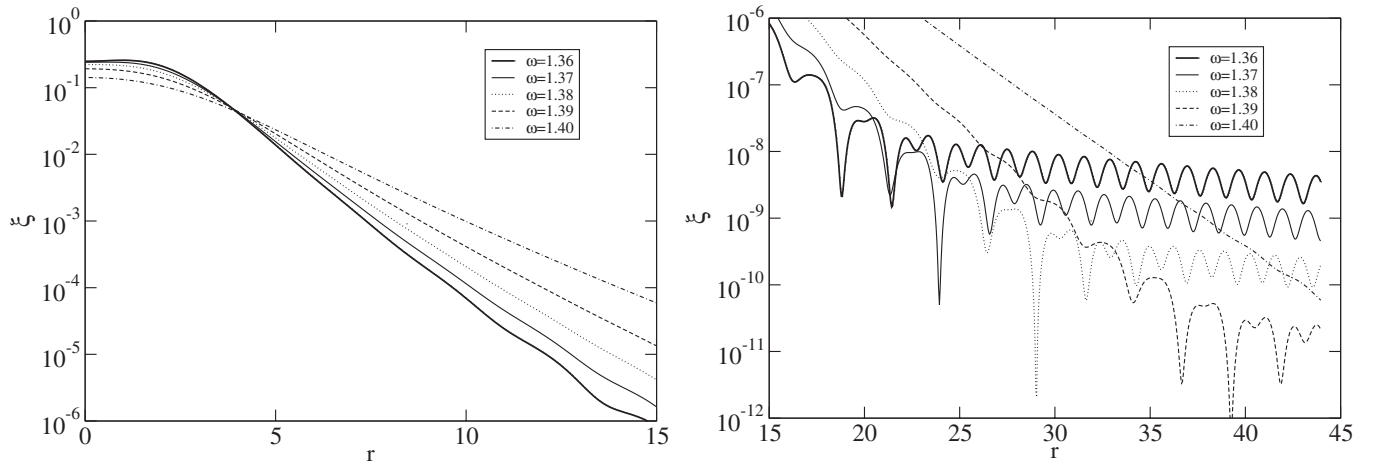


FIG. 15. Energy density for various values of  $\omega$ , near the origin (left panel) and in the region where the oscillatory tails dominate (right panel).  $R_{\text{lim}}$  is equal to 44.

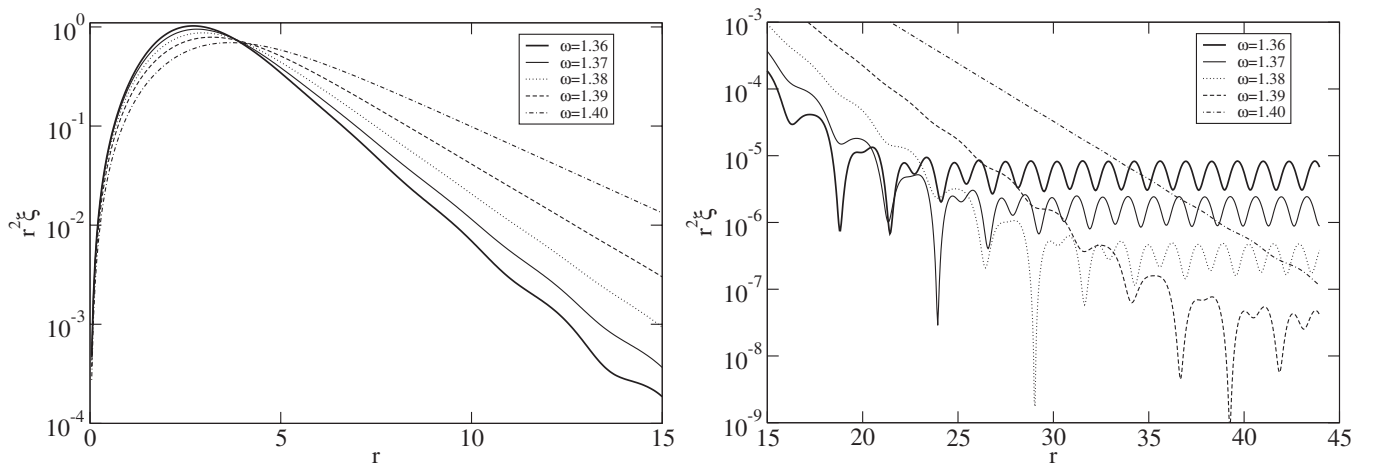


FIG. 16. Same as Fig. 15 but with the volume element included:  $r^2\xi$ .

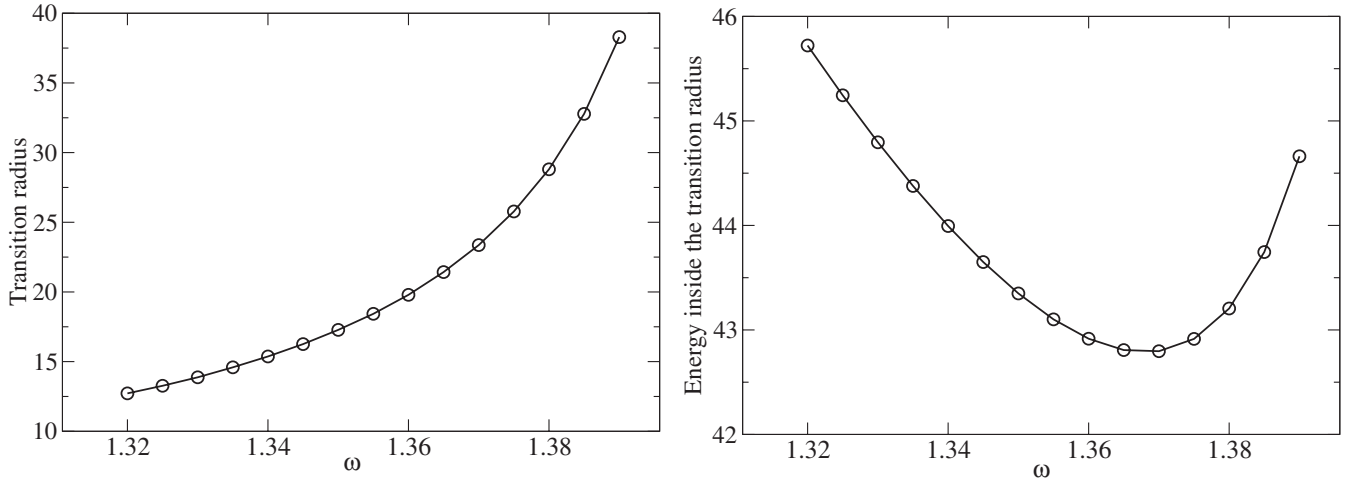


FIG. 17. The transition radius between the exponential decay and the oscillatory tail (left panel) and the energy inside this radius (right panel), as a function of  $\omega$ .

It is the radius at which the oscillatory behavior starts to dominate.  $R_{\text{trans}}$  as a function of  $\omega$  is shown on the left panel of Fig. 17. The precise location of the transition radius cannot be computed for  $\omega > 1.39$ , given our nominal choice for  $R_{\text{lim}} = 44$ . Once again, this illustrates the fact that, when going to higher values of  $\omega$ , one needs to increase the boundary radius  $R_{\text{lim}}$ . In the right panel of Fig. 17 we show the total energy inside the transition radius, i.e. the total energy of the core of the configuration. Contrary to the transition radius, this is not a monotonic function and there is a configuration of minimum energy. This nontrivial behavior is due to two competing effects when increasing  $\omega$ , first the increase of the transition

radius, and second the decrease of the magnitude of the modes. We also note that this minimum is very close to the value of the frequency which Honda and Choptuik [17] claim to be the one of their conjectured breather solution (i.e. they quoted  $\omega \approx 1.366$ ) but this may very well be just a coincidence. It seems likely that the energy contained in the core diverges when  $\omega \rightarrow \sqrt{2}$ .

Finally, in Fig. 18 we show the first modes near the origin (upper panels) and in the region of the transition radius (lower panels). Three different values of  $\omega$  are shown, corresponding to a low value (1.32), the value corresponding to the minimum of energy (1.365, cf. Fig. 17) and one rather high frequency (1.39).

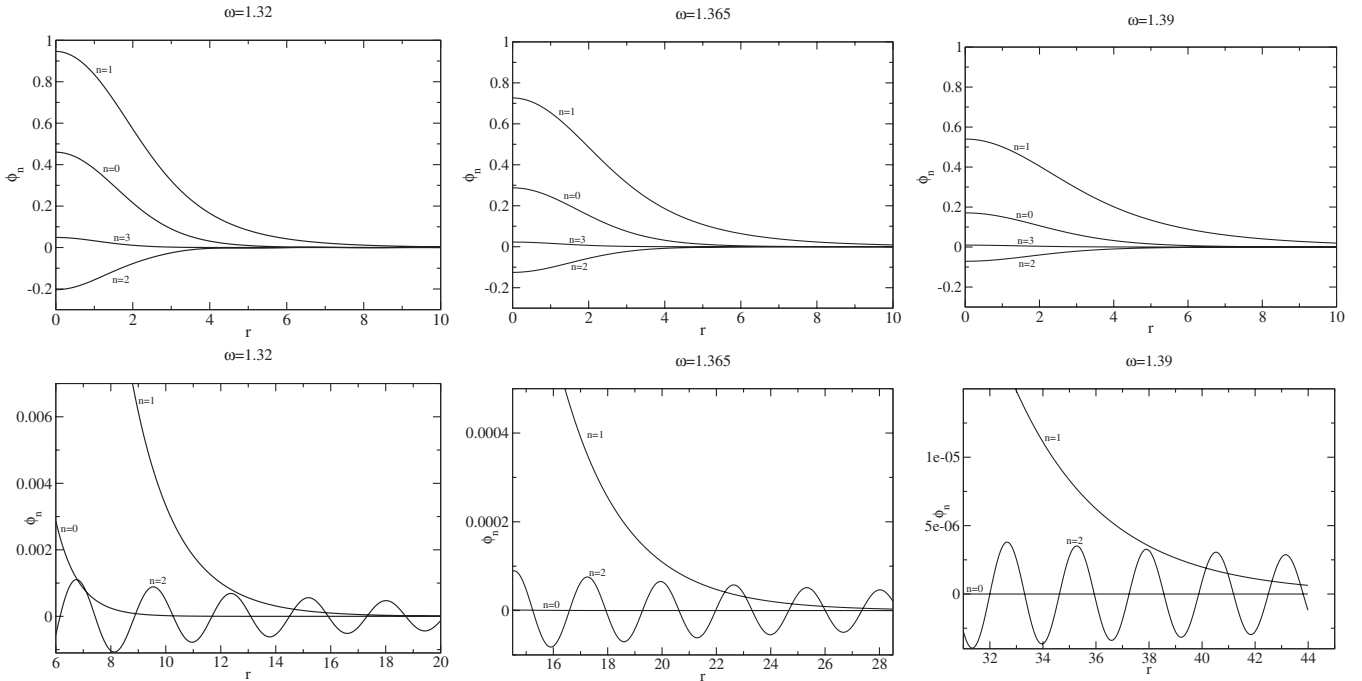


FIG. 18. The first modes near the origin and in the transition region for  $\omega = 1.32, 1.365, \text{ and } 1.39$ .

## VI. THE QUASIBREATHER CONTENT OF THE OSCILLONS

### A. Fourier decomposition of evolution results

In this section we present our oscillon scenario, based on the existence of the quasibreathers. In particular, we present some convincing evidence that an oscillon state of main frequency  $\omega$  is *quantitatively described* by a quasibreather of the same frequency, whose tail is cut off at some value of  $r$ . In order to do this we perform Fourier decomposition of various long-lived oscillon solutions found by doing the evolution (see Sec. II E for the actual method). This gives us the fundamental pulsation frequency  $\omega$  and the various modes. Then, those modes are compared to the ones found by directly solving the system (17) for this particular value of  $\omega$ . The same kind of comparison is done in Ref. [17] as to support the existence of a periodic solution of frequency  $\omega \approx 1.366$ . An important difference is that in Ref. [17] the comparison is performed only for higher frequency near-periodic states in an interval of  $[0 \leq r \leq 10]$  which is comparable to the core part of the quasibreather and therefore its oscillatory tail is not yet apparent.

It is apparent from the results provided by our evolution code that the solutions corresponding to the time evolution data are very close to being time symmetric not only at the center but also in the intermediately far region, justifying the choice of only cosine terms in the mode decomposition (16) when constructing QBs.

### B. Near-periodic states

First, we perform the Fourier decomposition of various near-periodic states obtained by fine-tuning the initial parameter  $r_0$ , since these states appear to be periodic and time symmetric to a very high degree. For a specific case, Figs. 19 and 20 show the real part of the modes coming from the Fourier transform of the evolution and the modes obtained by the direct solution of (17). The comparison is done with a near-periodic state corresponding to the first peak on the lifetime curve with initial data  $\phi_c = 1$ . The Fourier decomposition is performed between the two maxima at  $t_1 = 1592.29$  and  $t_2 = 1596.78$ . The frequency calculated from the position of the maxima is  $\omega = 1.398665$ , which is used to calculate the corresponding periodic solution by solving (17). The agreement for the first oscillating mode  $n = 2$  is remarkably good even in the oscillating tail region. The curves obtained by the two different decompositions are indistinguishable in the central region. In order to show the excellence of the agreement, the radial dependence of the relative difference of the corresponding modes obtained by the two methods is shown in Fig. 21. We have obtained similarly good agreement not only for  $\omega = 1.398665$  but for all frequencies for which near-periodic states exist (i.e. for  $1.365 < \omega < \sqrt{2}$ ).

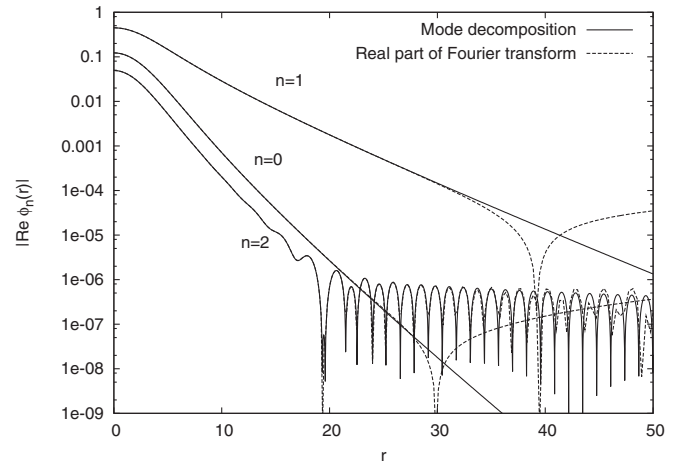


FIG. 19. Comparison between the modes coming from solving the system (17) directly and the real part of the modes obtained by performing a Fourier transform of the evolution for  $\omega = 1.398665$ . In order to be able to represent on the same graph the large values in the central oscillon region along with the small tails at high radii, the absolute values are plotted logarithmically. We note that the central value  $\phi_n(0)$  is positive for  $n = 0$  and for odd  $n$  while it is negative for other  $n$ . The peaks pointing downwards on the figure correspond to places where the functions change signature.

This comparison between the results coming from the evolution code of Sec. II and from the Fourier-mode decomposition of the quasibreathers is a very strong consistency check. Let us recall that the two codes have been developed completely independently.

Figure 22 shows, for large radii, the first mode for which the oscillatory term appears, i.e.  $\phi_2$ , in the case  $\omega = 1.38$ . It can be seen from the first of the three plots that the real part of the Fourier transform agrees very well with the decomposition of the corresponding QB, the two curves can hardly be distinguished. However, just at those radii

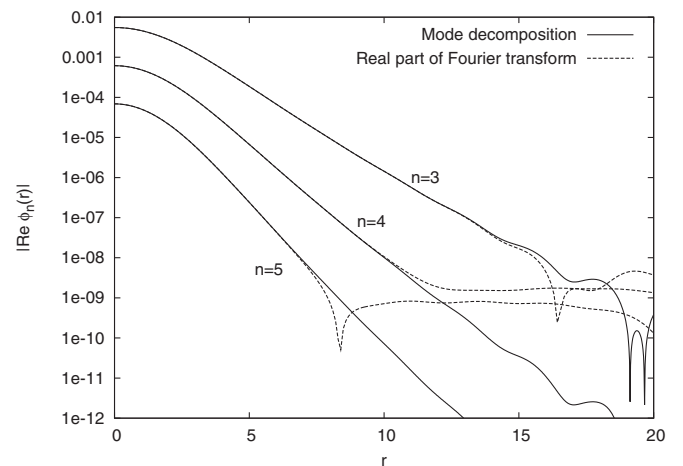


FIG. 20. Comparison of the higher modes of the two systems presented on the previous figure.

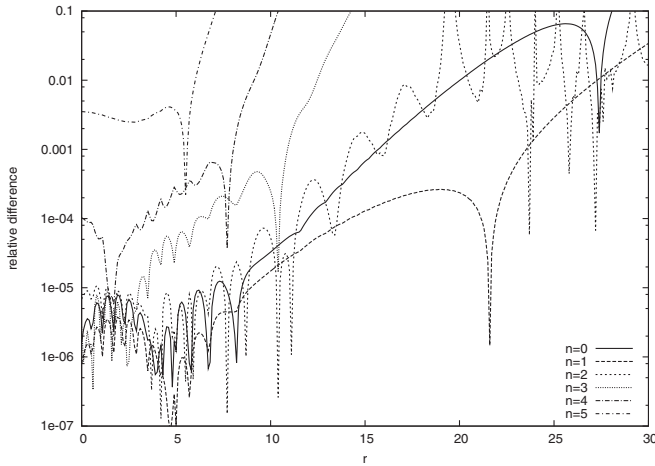


FIG. 21. Dependence on the radius  $r$  of the relative difference of the modes coming from the mode decomposition and the Fourier transformation for  $\omega = 1.398\,665$ . The relative difference is defined as the absolute value of the ratio of the difference and the mode decomposition value.

where the oscillatory behavior appears the imaginary part starts being comparable to the real part, breaking the time symmetry in this outer region. The second plot shows that

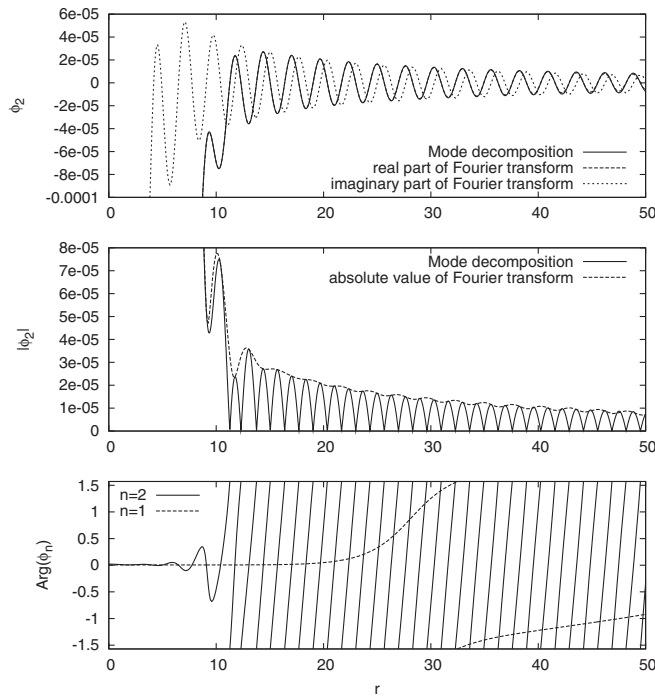


FIG. 22. The first two graphs compare the oscillatory region of the mode  $\phi_2$  coming from solving the system (17) directly and the complex  $\phi_2$  obtained by performing Fourier transform on the result of the evolution code, for  $\omega = 1.38$ . The first graph shows the real and imaginary parts separately, while the second compares the absolute values. The third graph plots the radial dependence of the complex argument of the modes  $\phi_1$  and  $\phi_2$  obtained by the Fourier transform.

the absolute value of the complex  $\phi_2$  obtained by the Fourier decomposition essentially behaves like a smooth envelope curve covering the standing wave like peaks of  $|\phi_2|$  obtained by the mode decomposition. The presence of the complex argument of the Fourier transform shown on the third plot indicates that the oscillating tail obtained by the evolution code is composed of outgoing waves carrying out energy from the core region.

### C. Oscillons from Gaussian initial data

Oscillons obtained by the evolution of generic Gaussian initial data are relatively long living for a large set of the possible values of the initial parameter  $r_0$ . In Fig. 23 we exhibit the time evolution of the frequency of the two typical non-fine-tuned states presented in Fig. 1. Although these states are clearly nonperiodic, their lifetime is still very large compared to the period of the basic high frequency oscillation mode. We have performed the Fourier decomposition of these states at various moments of time and compared the results to the mode decomposition of the corresponding QB. In Figs. 24–27 the Fourier decomposition of the two oscillon states shown in Figs. 1 and 23 is given for moments of time where the frequency is approximately 1.30 and 1.36. For comparison, the corresponding modes calculated by solving (17) using the given frequencies is also shown on the figures. Although the agreement of the modes is not as excellent as for the near-periodic states, the curves calculated by the two methods are still remarkably close. Especially important is the similarity at the tail section of the first oscillating mode, i.e. mode 2. This indicates that the periodic quasi-breather solutions can be used to describe, at least qualitatively, even the generic long living oscillons. In particular, the existence of the oscillating tail region is responsible for the slow but steady energy loss of these configurations.

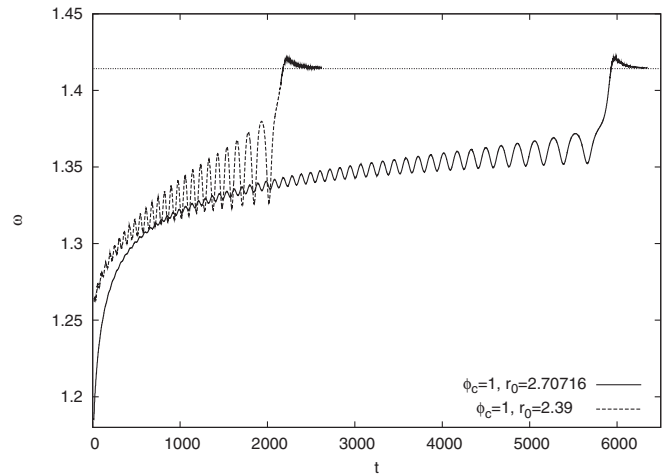


FIG. 23. Time evolution of the underlying high frequency oscillation of the oscillon state of Fig. 1 is presented.

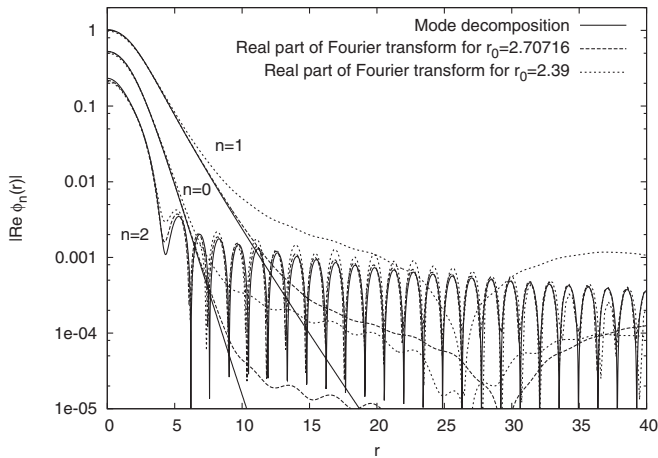


FIG. 24. The modes of the periodic solution with frequency 1.3 are compared with the Fourier decomposition of two different oscillon states. The first oscillon state with initial data  $\phi_c = 1$ ,  $r_0 = 2.70716$  is decomposed between the two subsequent maxima after  $t = 471.47$ , where the calculated frequency is 1.2995. The second state with  $\phi_c = 1$ ,  $r_0 = 2.39$  is decomposed just after  $t = 298.72$ , where the frequency is 1.3011.

**D. Initial data obtained by mode decomposition**

We have also tested our scenario in the reverse way. First, for a given  $\omega$  (1.38 in the first example), we have solved the system (17) for the modes of the quasibreather. In particular, we can compute  $\phi(t = 0)$  at the moment of time symmetry, and use this as initial data for the evolution code. The evolution of such initial data is shown in Fig. 28 for numerical simulation with various spatial resolutions. The field (here its value at the origin) oscillates at the appropriate frequency for a relatively long period (approximately  $t = 300$ , with about 66 oscillations) before it collapses in a subcritical or supercritical way very similar to the collapse of the  $\phi_c = -0.4$  states shown in Fig. 4. The initial state is so close to the ideal configuration that it even

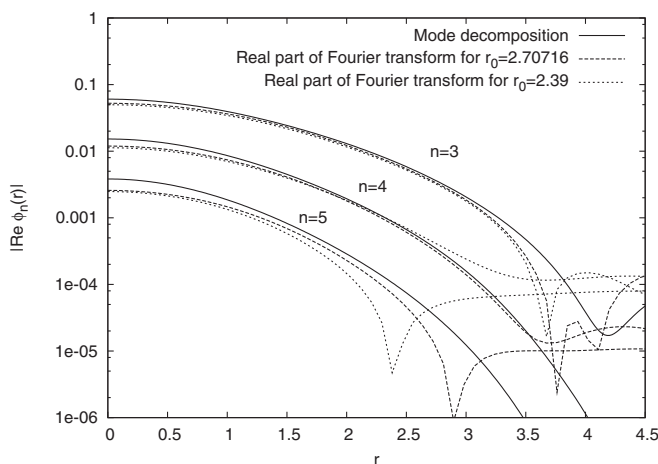


FIG. 25. Comparison of the higher modes of the two systems with frequency  $\omega = 1.3$  presented on the previous figure.

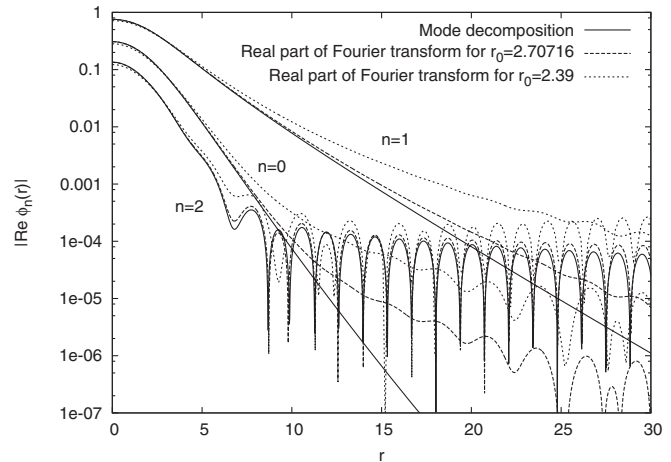


FIG. 26. The modes of the periodic solution with frequency 1.36 is compared with the Fourier decomposition of two different oscillon states. The first oscillon state with initial data  $\phi_c = 1$ ,  $r_0 = 2.70716$  is decomposed between the two subsequent maxima after  $t = 4158.76$ , where the calculated frequency is 1.3596. The second state with  $\phi_c = 1$ ,  $r_0 = 2.39$  is decomposed just after  $t = 1526.58$ , where the frequency is 1.3613.

depends on the chosen numerical resolution whether in the final stage the configuration collapses in a subcritical or supercritical way. Strangely, the longest living state is not the one with the highest resolution, which is probably connected to the fact that the initial data still contain small numerical errors. Although the lifetimes attainable by this method are very long compared to the dynamical time scale of the linearized problem, they are still shorter than the  $\tau \approx 2000$  achievable by fine-tuning the first peak of the  $\phi_c = -0.4$  initial data. Actually, it should not be surprising that the numerically determined initial data corresponding to a QB cannot be as long living as a configuration which is fine-tuned to 32 decimal digits.

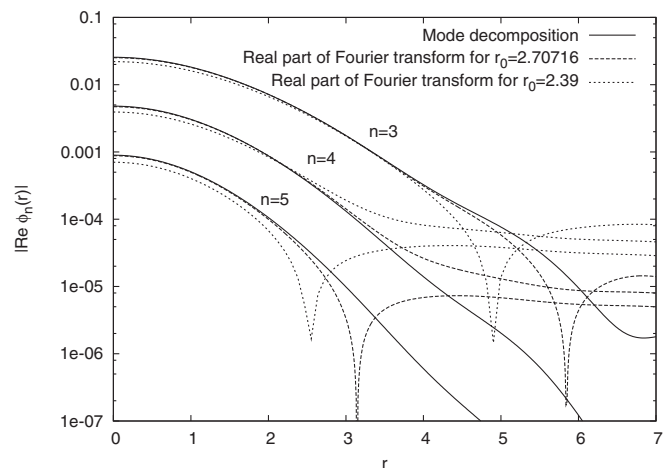


FIG. 27. Comparison of the higher modes of the two systems with frequency  $\omega = 1.36$  presented on the previous figure.

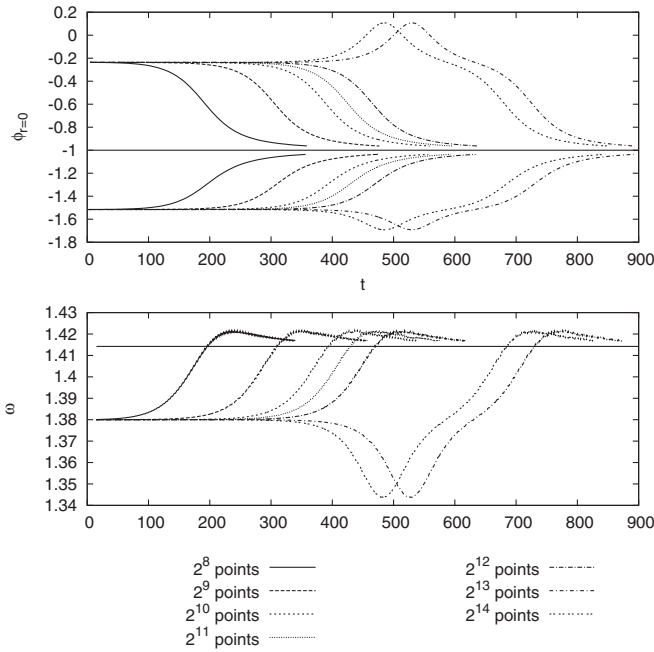


FIG. 28. On the first graph the upper and lower envelopes of the oscillations of the field at the origin are shown as functions of time for numerical simulations with various number of spatial grid points. The initial data is generated by solving the system (17) for the modes at the pulsation frequency  $\omega = 1.38$ . On the second graph the time dependence of the oscillation frequency is plotted for each simulation.

Since the modes are matched to oscillating tails at large radii, the initial data provided by the mode decomposition of a QB is valid up to arbitrarily large  $r$ . However, because of the slow falloff of the oscillating tails, the energy contained in balls of radius  $r$  diverges as  $r$  goes to infinity. Using such a configuration as initial data for our evolution code does not cause serious problems, since the physical distance between grid points in our numerical representation increases with the distance from the center, and consequently the high frequency tails cannot be represented numerically above a certain radius. This provides a cutoff in the initial configuration and an effective outer boundary during the evolution. An advantage of our conformal compactification method is that this outer boundary moves to higher and higher radii when increasing the numerical resolution. In Fig. 29 we show the initial part of the upper envelope curve for numerical runs with various spatial resolutions. We emphasize that this strong resolution dependence is entirely due to the inadequate representation of the infinite energy initial data. When we used initial data with compact support or sufficiently fast falloff, such as the Gaussian initial data in (12), then the code remained convergent up to much larger time periods (at the order of  $t = 10\,000$ ), and the curves with various resolutions agreed to very high precision at the initial stage (at around  $t = 100$ ).

An important point is that, with this method, we can generate almost periodic oscillons at frequencies which are

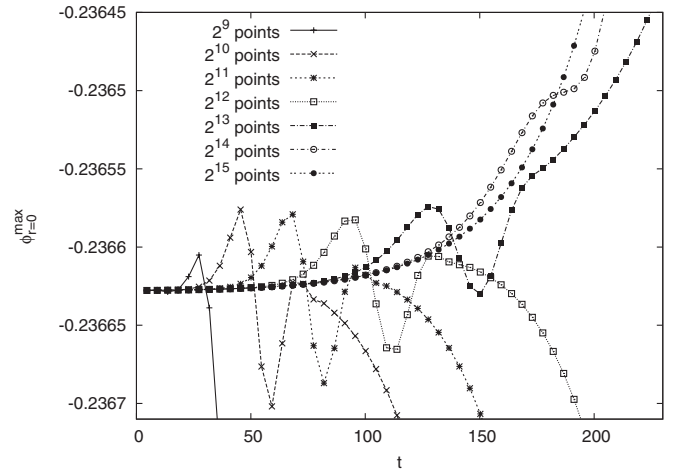


FIG. 29. Initial behavior of the maximum curve of the evolution of the  $\omega = 1.38$  initial data with numerical resolutions corresponding to various number of spatial grid points. The points on the curves represent the actual maximum points of the oscillating field  $\phi$  at the origin  $r = 0$ .

difficult or impossible to attain by fine-tuning initial data of the form (12). In Fig. 30 we show the upper envelope of the oscillations at  $r = 0$  in the initial stage of the evolutions when using initial data provided by the mode decomposition method with frequencies  $\omega = 1.30$  and  $\omega = 1.36$ . Again, as the numerical resolution is increased, the size of the oscillating tail that can be taken into account in the numerical representation of the initial data gets larger, and the evolution will remain nearly periodic for longer times. The field can oscillate truly periodically only if the energy lost by radiation through the dynamically oscillating tail is

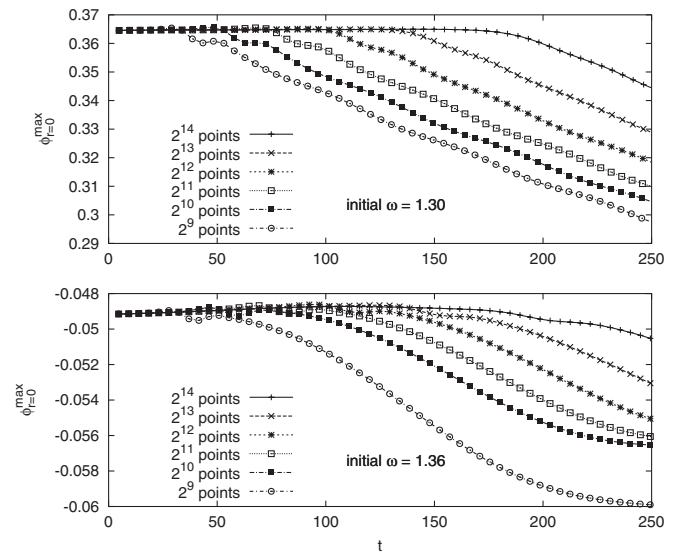


FIG. 30. Initial behavior of the upper envelope of the oscillations at  $r = 0$  of the evolution of the  $\omega = 1.30$  and  $\omega = 1.36$  initial data for numerical simulations with various number of spatial grid points.

balanced out by an incoming radiation already present at the tail section of the initial data. If the tail is cut off above some radius  $r$  then the nonperiodic region moves inwards from that radius essentially at the speed of light. Getting into the nonperiodic domain, for the frequencies  $\omega \leq 1.36$  the tail amplitude appears to be large enough to cause a small but significant energy loss, a decrease in amplitude, and consequently a steady frequency increase. In Figs. 31 and 32 we show the long-time behavior of the amplitude and frequency of the oscillations generated by initial data with frequencies  $\omega = 1.30$  and  $\omega = 1.36$ . Apart from a relatively short stable initial stage, the main characteristic of the evolution is a slow but steady decrease of the amplitude accompanied by a simultaneous increase of the frequency up to a point (approximately  $\omega = 1.365$ ) where the configuration quickly decays. This evolution is very similar to the behavior of generic (i.e. not fine-tuned) oscillons started from Gaussian initial data of type (12). A typical example of such evolution, with initial data corresponding to an  $r_0$  close to the top of the lifetime curve (but between two peaks) with  $\phi_c = 1$ , is also shown in Figs. 31 and 32 in order to facilitate comparison. It is also rather remarkable that the onset of the rapid decay seems to coincide with the configuration which minimizes the energy inside the core (see Fig. 17).

The long-time evolution of a low frequency initial data provided by the mode decomposition method is very similar to the evolution of generic oscillons evolving from Gaussian initial data. An important difference though is the smaller low frequency modulation of the envelope curve and of the time dependence of the frequency. From this, one can expect that the Fourier decomposition of these states is even closer to that of the quasibreather state with

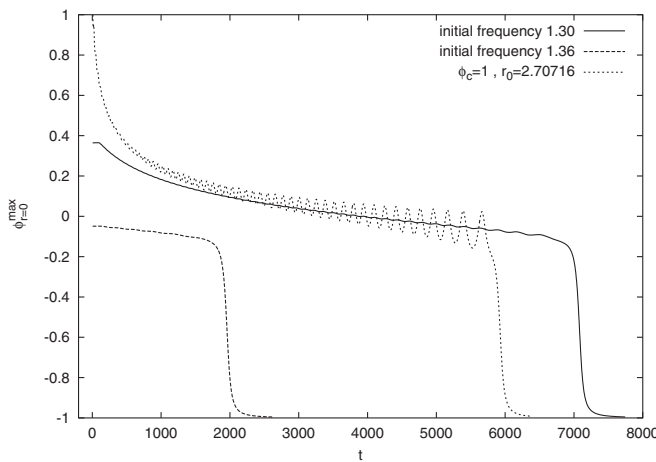


FIG. 31. Time evolution of the upper envelope curve of the oscillation of  $\phi$  at  $r = 0$  generated by three different initial data. The first two initial data are provided with the mode decomposition method, solving the system (17) by choosing the frequencies  $\omega = 1.30$  and  $\omega = 1.36$ . The third evolution corresponds to Gaussian-type initial data (12) with  $\phi_c = 1$  and  $r_0 = 2.70716$ .

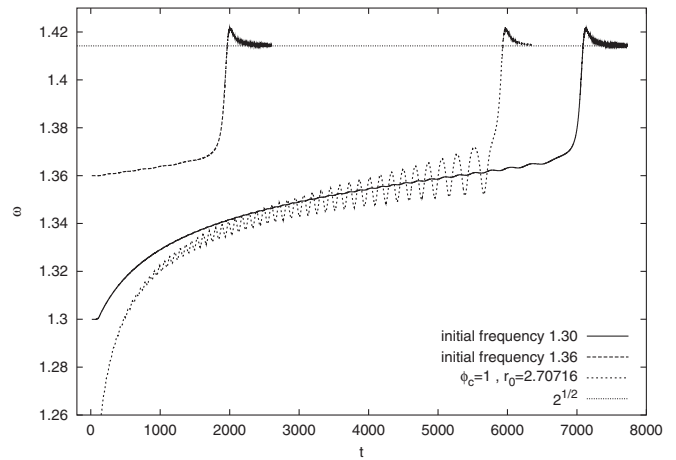


FIG. 32. Time evolution of the frequency of the oscillation of  $\phi$  at  $r = 0$  for the three kinds of evolution simulations shown on the previous figure.

the corresponding frequency. In Figs. 33 and 34 we give the Fourier decomposition of the evolution of the 1.3 initial data between the two maxima after  $t = 5257.45$ , where the calculated frequency is 1.35997. The agreement is markedly better than in Figs. 26 and 27, which is most likely due to the much lower amplitude of the low frequency modulations on the envelopes of field value at the center. These low frequency modes are excited to a higher amplitude by the Gaussian type of initial data, while they appear to be present to a much lower extent in the lower frequency periodic initial data (with  $\omega = 1.3$  in this case). We remind the reader that the existence of the peaks on the lifetime curve (see Fig. 4 of [17]) is closely related to these low frequency oscillations. Namely, the peaks separate do-

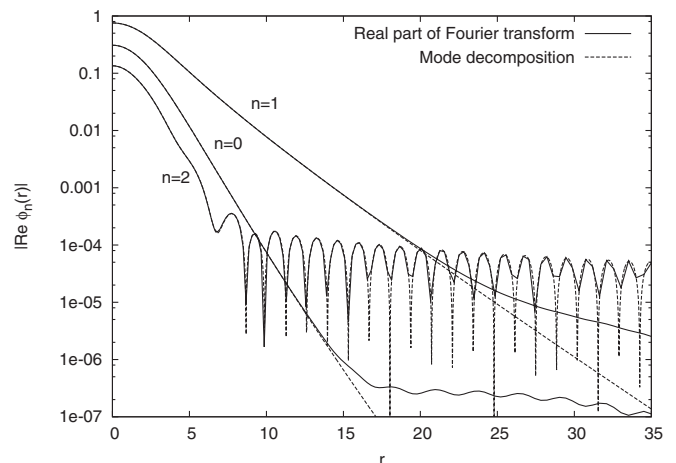


FIG. 33. Fourier decomposition of the evolution of the  $\omega = 1.3$  initial data close to the moment of time when its frequency increases to 1.36. The results are compared to the modes of the periodic solution obtained by the mode decomposition method for the  $\omega = 1.36$  frequency.

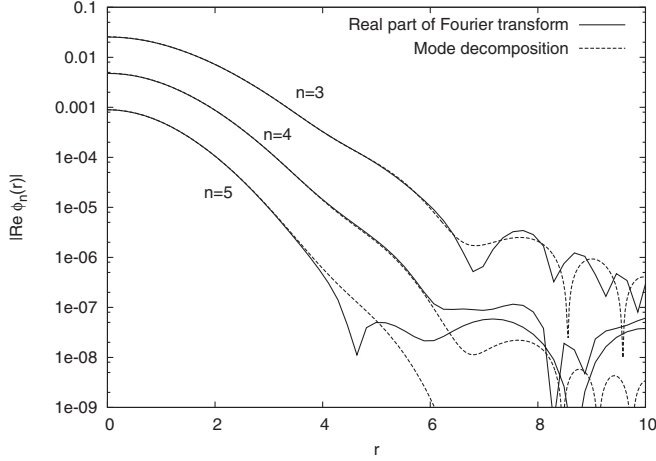


FIG. 34. Same thing as Fig. 33 but for the higher order modes.

mains of the initial data in  $r_0$  with a different number of low frequency oscillations on the envelope curve.

### E. Virialization properties

Since the solutions are close to being periodic, it appears to be worthwhile to apply a virial approach introduced in [9]. The virial equation can be obtained by multiplying the nonlinear wave equation (3) by  $2\pi r^2 \phi$ , integrating over a radial domain  $0 < r < r_b$ , and then averaging for a time period  $t_0 < t < t_1$ . Taking into account boundary terms, one obtains

$$\begin{aligned} \langle E_k \rangle - \langle E_s \rangle - 2\pi \left\langle \int_0^{r_b} dr r^2 \phi^2 (\phi^2 - 1) \right\rangle \\ = \frac{2\pi}{t_1 - t_0} \int_0^{r_b} dr [(\phi \partial_t \phi)_{t_1} - (\phi \partial_t \phi)_{t_0}] \\ - 2\pi \langle (r^2 \phi \partial_r \phi)_{r_b} \rangle, \end{aligned} \quad (23)$$

where

$$E_k = \int_0^{r_b} dr (\partial_t \phi)^2, \quad E_s = \int_0^{r_b} dr (\partial_r \phi)^2 \quad (24)$$

are the kinetic and surface energies, respectively, and the time averaging is defined as

$$\langle \rangle = \frac{1}{t_1 - t_0} \int_{t_0}^{t_1} dt. \quad (25)$$

The left-hand side of Eq. (23) is the ‘‘departure from virialization’’ introduced in [9]. It is exactly zero when the boundary terms on the right side are vanishing. If the configuration is exactly periodic then the first term on the right-hand side is zero, while  $\lim_{r_b \rightarrow \infty} r^2 \phi \partial_r \phi = 0$  ensures that the second term also vanishes asymptotically.

Since the exactly periodic quasibreather configurations contain infinite energy in the tails,  $E_k$  and  $E_s$  increases unboundedly when  $r \rightarrow \infty$ , and the virial equation can be considered only for a finite radius domain. Furthermore,

for large radius  $\phi$  is dominated by the oscillating tail of mode  $n = 2$ , i.e.  $\phi \approx A_2 \cos(2\omega t) \sin(|\lambda_2| r)/r$ . Consequently, the time average of the outer boundary term for large  $r_b$  behaves like  $2\pi \langle (r^2 \phi \partial_r \phi)_{r_b} \rangle = \pi A_2^2 |\lambda_2| \sin(2|\lambda_2| r_b)/2$ , not tending to zero at infinity. Since the boundary term oscillates around zero, by averaging in a spherical shell  $[r_b - \delta r, r_b + \delta r]$  the departure from virialization tends to zero when  $\delta r \gg |\lambda_2|$ . This means that, although the quasibreather solutions are strictly periodic, they are virialized only in a radially averaged sense.

We have shown in the previous subsections that the core part of oscillons agree to a very high precision to the core of the corresponding quasibreather. For larger radii, the first essential difference that arises is in the phase of the oscillating tail. As illustrated in Fig. 22, the oscillon contains a component  $\sim A_2 \sin(2\omega t)$ , related to the fact that the oscillons radiate. In this case the asymptotic behavior of the field is  $\phi \approx A_2 \sin(2\omega t - |\lambda_2| r)/r$ , and consequently the dominant part of the time average of  $r^2 \phi \partial_r \phi$  will be independent of the radial coordinate. The departure from virialization will be proportional to  $A_2^2$ , consistently with the picture that the loss of energy of the oscillon is proportional to the squared amplitude of the tail. In Fig. 8 the dependence of  $A_2$  on the frequency is shown, indicating that the closer the frequency is to  $\sqrt{2}$  the smaller is the departure from the virialization, corresponding to longer oscillon lifetime.

## VII. CONCLUSION

In this paper, we have adapted and applied spectral methods implemented in the LORENE library to find time-periodic solutions of the spherically symmetric wave equation of  $\phi^4$  theory. Our code passed numerous tests and we are quite confident that it is sufficiently precise. With our code we find that for frequencies  $0 < \omega < \sqrt{2}$  there is a whole family of standing wave-type solutions with a regular origin having a well localized core and an oscillatory tail. Because of the slow decrease of the oscillatory tail the total energy of these solutions in a ball of sufficiently large radius,  $R$ , is proportional to  $R$  (cf. Figs. 15 and 16). We have constructed a special class of solutions, called quasibreathers, defined by minimizing the amplitude of the oscillatory tail of the solutions. The size of the core of the QBs gets larger and larger as  $\omega \rightarrow \sqrt{2}$  and the amplitude of the oscillatory tail is getting smaller and smaller. Interestingly, the energy contained in the core of the QBs exhibits a minimum for  $\omega \approx 1.365$ .

Using our high precision time evolution code, we have also investigated the time evolution of Gaussian initial data. We observe that a generic oscillon state can be characterized by a slowly varying frequency,  $\omega(t)$ , increasing in time up to a critical one  $\omega_c$ , when it decays rapidly. We have also investigated in detail the near-periodic states described first in Ref. [17] which can be characterized by

an almost constant frequency. In contradistinction to Ref. [17], we find such near-periodic states for any frequency  $\sqrt{2} > \omega > \omega_c$ . Moreover, we find that the near-periodic states decay in time (i.e. they cannot be truly time-periodic states) (cf. Figs. 5 and 6). In particular, while losing some of their energy their frequency decreases very slowly with time.

By a careful comparison of the Fourier modes of an oscillon state of frequency  $\omega(t)$  with that of the corresponding QB, we have obtained convincing evidence that the localized part of the oscillon is nothing but the core of the QB of the same frequency. Our results demonstrate that the time evolution of an oscillon state can be described to a good approximation as an adiabatic evolution through a sequence of QBs with a slowly changing frequency  $\omega(t)$ . What is more, the oscillatory tail of the QB describes very well the standing wave part of the oscillon. Therefore any oscillon contains the core and a significant part of the

oscillatory tail of the corresponding QB. The existence of near-periodic states is closely related to the fact that the energy of the oscillon core exhibits a minimum for a critical frequency  $\omega_c \approx 1.365$  and for  $\sqrt{2} > \omega > \omega_c$  a single unstable mode appears which can be suppressed by fine-tuning the initial data.

After completion of the manuscript our attention has been drawn to the unpublished work of Watkins [37] discussing related ideas.

## ACKNOWLEDGMENTS

This research has been supported by OTKA Grants No. T034337, No. TS044665, and No. K61636, and by the Pole Numerique Meudon-Tours. G. F. and I. R. would like to thank the Bolyai Foundation for financial support. We would like to thank P. Salmi for providing us with a copy of Watkins' unpublished work [37].

- 
- [1] N. S. Manton and P. Sutcliffe, *Topological Solitons* (Cambridge University Press, Cambridge, England, 2004).
  - [2] R. F. Dashen, B. Hasslacher, and A. Neveu Phys. Rev. D **11**, 3424 (1975).
  - [3] A. E. Kudryavtsev, JETP Lett. **22**, 82 (1975).
  - [4] H. Segur and M. D. Kruskal, Phys. Rev. Lett. **58**, 747 (1987).
  - [5] P. A. Vuillermot, Comm. Math. Helv. **64**, 573 (1987).
  - [6] J. P. Boyd, *Weakly Nonlocal Solitary Waves and Beyond-All-Orders Asymptotics* (Kluwer, Amsterdam 1998).
  - [7] I. L. Bogolubskii and V. G. Makhankov, JETP Lett. **24**, 12 (1976); **25**, 107 (1977).
  - [8] M. Gleiser, Phys. Rev. D **49**, 2978 (1994).
  - [9] E. J. Copeland, M. Gleiser, and H.-R. Müller, Phys. Rev. D **52**, 1920 (1995).
  - [10] M. Gleiser Phys. Lett. B **600**, 126 (2004).
  - [11] E. Farhi, N. Graham, V. Khemani, R. Markov, and R. Rosales, Phys. Rev. D **72**, 101701(R) (2005).
  - [12] M. Gleiser, hep-th/0602187.
  - [13] I. Dymnikova, L. Koziel, M. Khlopov, and S. Rubin, Gravitation Cosmol. **6**, 311 (2000).
  - [14] N. Graham and N. Stamatopoulos, Phys. Lett. B **639**, 541 (2006).
  - [15] B. Piette and W. J. Zakrzewski, Nonlinearity **11**, 1103 (1998).
  - [16] M. Hindmarsh and P. Salmi, Phys. Rev. D **74**, 105005 (2006).
  - [17] E. P. Honda and M. W. Choptuik, Phys. Rev. D **65**, 084037 (2002).
  - [18] E. P. Honda, Ph.D. thesis, The University of Texas at Austin, 2000, hep-ph/0009104.
  - [19] S. Flach and C. R. Willis, Phys. Rep. **295**, 181 (1998).
  - [20] G. Fodor and I. Rácz, Phys. Rev. Lett. **92**, 151801 (2004).
  - [21] G. Fodor and I. Rácz, hep-th/0609110.
  - [22] A. B. Adib, M. Gleiser, and C. A. S. Almeida, Phys. Rev. D **66**, 085011 (2002).
  - [23] R. Courant and D. Hilbert, *Methods of Mathematical Physics* (Interscience Publishers, New York, 1962).
  - [24] B. Gustafsson, H.-O. Kreiss, and J. Olinger, *Pure and Applied Mathematics* (Wiley, New York, 1995).
  - [25] M. Gleiser and A. Sornborger, Phys. Rev. E **62**, 1368 (2000).
  - [26] G. Fodor and I. Rácz, Phys. Rev. D **68**, 044022 (2003).
  - [27] Y. Hida, X. S. Li, and D. H. Bailey, Lawrence Berkeley National Laboratory Report No. LBNL-46996, 2000. See and download at <http://crd.lbl.gov/~dhbailey/mpdist/index.html>.
  - [28] Webpage: <http://www.lorene.obspm.fr>.
  - [29] P. Grandclément, S. Bonazzola, E.ourgoulhon, and J.-A. Marck, J. Comput. Phys. **170**, 231 (2001).
  - [30] J. Novak and S. Bonazzola, J. Comput. Phys. **197**, 186 (2004).
  - [31] A. Sommerfeld, *Partial Differential Equations in Physics* (Academic Press, New York, 1949).
  - [32] S. Bonazzola, E.ourgoulhon, P. Grandclément, and J. Novak, Phys. Rev. D **70**, 104007 (2004).
  - [33] The Gnu Scientific library. Webpage: <http://www.gnu.org/software/gsl>.
  - [34] J. A. Nelder and R. Mead, Comp. J. **7**, 308 (1965).
  - [35] E.ourgoulhon, P. Grandclément, K. Taniguchi, J.-A. Marck, and S. Bonazzola, Phys. Rev. D **63**, 064029 (2001).
  - [36] J. M. Coron, C.R. Acad. Sci. Paris I **294**, 127 (1982).
  - [37] R. Watkins, DART-HEP-96/03, 1996.